CHAPTER 3

Solution-State Dynamic Nuclear Polarization

Mark D. Lingwood and Songi Han¹

Contents	1. Introduction	84
	2. Theoretical Background	86
	2.1. NMR signal enhancement through the	
	Overhauser effect	86
	2.2. DNP parameters	89
	2.3. Modelling the coupling factor	92
	3. Experimental Results	96
	3.1. Measuring the coupling factor	96
	3.2. Low magnetic fields: Below 0.1 T	100
	3.3. Magnetic fields corresponding to X-band ESR:	
	0.3-0.35 T	107
	3.4. High magnetic fields: Above 1 T	111
	3.5. DNP with flowing or shuttling between fields	114
	3.6. Proton–electron double resonance imaging	117
	4. Conclusion	120
	References	120

Abstract

Solution-state dynamic nuclear polarization (DNP) is an increasingly popular method of enhancing nuclear spin polarization that has many applications in nuclear magnetic resonance (NMR) and magnetic resonance imaging (MRI). The theory, methods and applications of DNP in the solution state using the Overhauser effect are distinctly different from those of solid-state DNP or what is known as dissolution DNP. This review discusses the theory and recent experimental advances of Overhauser DNP techniques in the

Department of Chemistry and Biochemistry, University of California, Santa Barbara, California, USA $^{\rm 1}$ Corresponding author.

solution state at various field strengths ranging from the earth's magnetic field to 9.2 T, covering the literature from 1986 to late 2010. Most of the focus in this review is on spectroscopy applications of DNP, although proton—electron double resonance imaging (PEDRI) and remotely enhanced liquids for imaging contrast (RELIC) applications are briefly covered.

Key Words: Dynamic nuclear polarization, DNP, Overhauser effect, Hyperpolarization, Sensitivity enhancement, Hydration dynamics, Portable NMR, PEDRI, Overhauser MRI, RELIC.

1. INTRODUCTION

Magnetic resonance techniques have found many key applications in a diverse range of fields from structural identification to medical imaging, owing to the wealth of available information at the molecular level and the non-invasive nature of the technique. However, while nuclear magnetic resonance (NMR) and magnetic resonance imaging (MRI) are powerful approaches, they are also inherently insensitive. The small energy splitting between nuclear spin states even in a strong magnetic field results in low thermal polarization of the nuclei (due to Boltzmann statistics), and only a fraction of the nuclei contribute to the observed signal. This problem is compounded for elements that have a low natural abundance of magnetically active nuclei, such as the biologically important ¹³C and ¹⁵N.

One way to overcome the insensitivity of NMR and MRI is to increase the applied magnetic field, as the Zeeman splitting of the nuclear spin states increases with magnetic field. Currently, the highest commercially available magnet for NMR is 23.5 T, but even this very high field strength only gives ¹H nuclear polarizations of 0.008% at room temperature. High magnetic fields also do not solve another difficulty of magnetic resonance, namely the often very limited contrast between the signal of interest and the background signal. This is especially true for MRI, where for some applications, the naturally available signal contrast is not sufficient for image interpretation, and therefore external contrast agents must be added to the sample.

These limitations of sensitivity and contrast have led researchers to develop hyperpolarization methods, where the nuclear polarization is greatly increased by the manipulation of spin states. Currently, the most general and popular hyperpolarization method is dynamic nuclear polarization (DNP), where the much higher polarization of an unpaired electron is transferred to the nuclei of interest. DNP was originally

predicted in 1953 by Albert Overhauser for conduction electrons, and was soon experimentally verified by Carver and Slichter. Further investigation found that DNP was not only effective for metals, but could also be applied to diamagnetic crystals and paramagnetic molecules in solution. DNP experiments can be performed in the liquid state through the Overhauser effect. or in the solid state through the solid effect, thermal mixing or cross effect. Solid-state DNP can give very large enhancements at cryogenic temperatures, and the combination of DNP at 1.2 K and rapid sample dissolution to ambient temperatures (which is known as dissolution DNP) can give up to 10,000-fold signal enhancement for molecules in solution. The recent commercial availability of dissolution DNP equipment has helped to spur the general growth of all DNP approaches.

There are several distinct advantages to performing DNP directly in the solution state. While the achievable enhancements in liquids are smaller than what is possible through dissolution DNP, the equipment is often much simpler and the sample does not have to undergo a freeze—thaw process. Most importantly, many applications do not depend on the ultimate signal gain but instead draw information from the contrast provided by the electron—nuclear interaction, and thus provide unique information about molecular properties, interactions and interfaces, giving insight into materials and biological systems and presenting new opportunities. The enhancement levels available with Overhauser DNP are still significant and can enhance detection sensitivity, allow the observation of previously undetectable species and enable faster signal acquisition.

In this review, we focus on solution-state DNP studies utilizing the Overhauser effect. Solid-state DNP is not included in this review, ^{9,10} nor are experiments where the hyperpolarization is performed in the solid state before melting ^{11,12} or dissolving ^{8,13,14} the sample into solution. Chemically induced DNP (CIDNP) ^{15–17} and the Overhauser effect of conduction electrons ^{18,19} are also excluded, and the interested reader is referred to the cited papers for more information. The principles and prospects of proton–electron double resonance imaging (PEDRI) are briefly included, as a thorough coverage of this research area is out of the scope of this document.

This review attempts to include all solution-state DNP papers from 1986 to late 2010. While solution-state DNP has been reviewed as recently as 1993, ²⁰ we chose to cover a slightly larger time frame as it encompasses the modern renaissance of DNP. For earlier papers, the reader is referred to a number of excellent reviews. ^{4,20–22} Interestingly, the number of papers discussing solution-state DNP has dramatically increased even during the past 3 years, as can be seen in Figure 1. This chart implies that solution-state DNP is a rapidly expanding field with a strong future ahead.

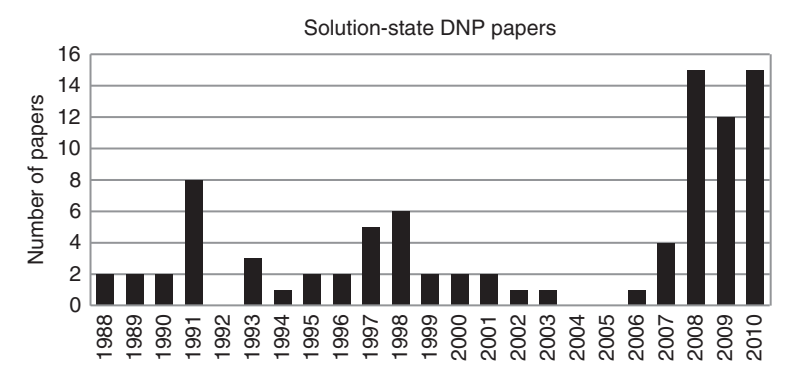


Figure 1 Experimental solution-state DNP papers cited in this work, displayed by the year of publication. Papers with PEDRI results are not included in this chart because only selected PEDRI papers are cited in this review.

2. THEORETICAL BACKGROUND

The Overhauser effect has been widely employed as an NMR analysis method in many disciplines ranging from medical to chemical sciences, and broadly refers to the motion-mediated transfer of spin polarization from a species with a higher gyromagnetic ratio (γ) to one with a lower gyromagnetic ratio. Because molecular motion is critical for efficient transfer, the Overhauser effect is most commonly observed in liquid samples. The Overhauser effect can be divided into two categories: the nuclear Overhauser effect (NOE), where both species are nuclear spins, and Overhauser DNP, where the higher γ spin is an unpaired electron. As Overhauser DNP is the focus of this review, some of the terminology and equations are specific to the Overhauser DNP effect.

2.1. NMR signal enhancement through the Overhauser effect

The Hamiltonian for a system of two coupled spin 1/2 species I and S in a magnetic field is given by⁴

$$\mathcal{H} = \hbar \gamma_{S}(\mathbf{S} \cdot \mathbf{B}_{0}) + \hbar \gamma_{I}(\mathbf{I} \cdot \mathbf{B}_{0}) + \mathcal{H}_{S} + \mathcal{H}_{D}. \tag{1}$$

The first and second terms describe the electron and nuclear Zeeman interactions, where γ_S and γ_I are the gyromagnetic ratios of the electron and nucleus, respectively, and \mathbf{B}_0 is the externally applied magnetic field. This description of the electron Zeeman interaction is appropriate for a free electron or organic radical, but for metal ions or semiconductors it should be rewritten as $g\mu_B(\mathbf{S} \cdot \mathbf{B}_0)$ where g is the g-factor of the unpaired electron and μ_B is the Bohr magnetron. The terms \mathcal{H}_S and \mathcal{H}_D in

Equation (1) represent, respectively, the scalar and dipolar interactions between the electron and nucleus and are given by

$$\mathcal{H}_{S} = \frac{\gamma_{S} \gamma_{I} \hbar^{2} 8\pi}{3} |\psi(0)|^{2} (\mathbf{I} \cdot \mathbf{S})$$
 (2a)

$$\mathcal{H}_{D} = \gamma_{S} \gamma_{I} \hbar^{2} \left[\frac{\mathbf{I} \cdot \mathbf{S}}{r^{3}} - \frac{3(\mathbf{I} \cdot \mathbf{r})(\mathbf{S} \cdot \mathbf{r})}{r^{5}} \right]$$
 (2b)

The scalar interaction is proportional to the square of the unpaired electron's wavefunction at the nucleus, $|\psi(0)|^2$. In general, this quantity is not known or cannot be determined, making the scalar interaction difficult to predict except in certain and simple situations.⁴ The dipolar term is heavily dependent on the distance r between the two spins, leading to the distance (and time) dependence of the Overhauser effect. Further discussions of the dipolar interaction term are available in the literature.²³

At fields above ~ 100 mT, the scalar and dipolar terms are small relative to the Zeeman terms and they can be treated as perturbations to describe the system with the four-level energy diagram shown in Figure 2. Saturation of the electron spin resonance (ESR) transition p will create a non-equilibrium population distribution in the system if cross-relaxation occurs through the transitions w_0 and w_2 . This causes the nuclear spin polarization to be increased, as long as $w_0 \neq w_2$. In the limit of pure dipolar coupling, relaxation through w_2 is six times greater than

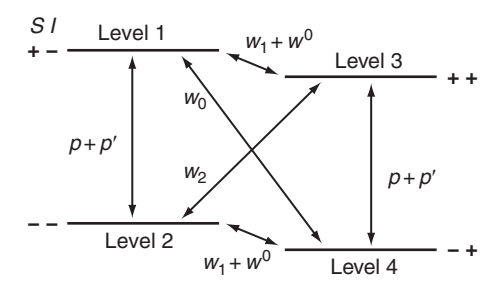


Figure 2 The four-level diagram for a system of two interacting spins, in this case an electron (S) and nucleus with a positive gyromagnetic ratio (I). The intrinsic electron and nuclear spin relaxation are given by p and w^0 , respectively, and the dipolar and/or scalar interactions between the electron and nuclear spin are represented by p', w_0 , w_1 and w_2 . The transition w_0 is known as the zero-quantum transition, while w_1 is the single-quantum transition and w_2 is the double-quantum transition. Nuclear and electronic relaxation through mechanisms other than scalar or dipolar coupling are denoted with $w^0 = 1/T_{10}$ and $p = 1/T_{1e}$, where T_{10} and T_{1e} are the longitudinal relaxation times of the nucleus and electron in the absence of any coupling between them. Since much stronger relaxation mechanisms are available to the electron spin, the assumption $p \gg p'$ can be safely made. Adapted with permission from Ref. [24].

that through w_0 ,²⁵ which results in an increased population of the higher energy nuclear spin state giving an enhanced NMR signal that is in the opposite phase as the non-enhanced signal. Pure scalar coupling occurs if the relaxation is exclusively through w_0 , and produces an enhanced NMR peak in the same phase as the thermally polarized signal. The mutual spin relaxation transitions w_0 and w_2 require an exchange of energy with the lattice, and thus these transitions are effective only if the dipolar and scalar terms in the Hamiltonian are time dependent on a timescale comparable to the inverse of the electron Larmor frequency, which is ~ 100 ps (1/10 GHz) at 0.35 T.⁶ Either translational or rotational motion can satisfy this time dependence; for example, the translational motion of two colliding small molecules in a liquid is characterized by correlation times on the order of 100 ps, ²⁶ while the rotational motion of a complex of two small molecules can have correlation times on the order of 10 ps.^{26,27}

The mathematical formulation for Overhauser DNP comes from the differential equation for population changes of the nuclear spin state I, from the initial value I_0 to the excited value $\langle I_z \rangle$, originally described by Solomon²⁸:

$$\frac{\mathrm{d}\langle I_z \rangle}{\mathrm{d}t} = -(w_0 + 2w_1 + w_2 + w^0)(\langle I_z \rangle - I_0) - (w_2 - w_0)(\langle S_z \rangle - S_0)$$
 (3)

There is a similar equation for the electron spin S, but it can be ignored in this context due to the more powerful intrinsic relaxation processes of an electron spin. Since we want to know the steady state populations of the detected nuclear spin I, $d\langle I_z\rangle/dt$ can be set to zero and solved, giving Equation (4)

$$\frac{\langle I_z \rangle}{I_0} = 1 + \frac{w_2 - w_0}{w_0 + 2w_1 + w_2} \cdot \frac{w_0 + 2w_1 + w_2}{w_0 + 2w_1 + w_2 + w^0} \cdot \frac{S_0 - \langle S_z \rangle}{S_0} \cdot \frac{S_0}{I_0}. \tag{4}$$

Equation (4) is written in a form that best presents the physical parameters that describe DNP enhancements. The following definitions:

$$\rho = \frac{w_2 - w_0}{w_0 + 2w_1 + w_2} \tag{5a}$$

$$f = \frac{w_0 + 2w_1 + w_2}{w_0 + 2w_1 + w_2 + w^0}$$
 (5b)

$$s = \frac{S_0 - \langle S_z \rangle}{S_0} \tag{5c}$$

are used in order to rewrite Equation (4) to give the primary equation describing DNP enhancement,

$$E = \frac{\langle I_z \rangle}{I_0} = 1 - \rho f s \frac{|\gamma_S|}{\gamma_I}.$$
 (6)

In Equations (4) and (6), E is the observed signal enhancement obtained from the signal integral before and after electron spin saturation, ρ is the coupling factor, f is the leakage factor and s is the saturation factor. In Equation (6), the negative gyromagnetic ratio of the electron is factored out to give a negative sign in front of the second term. Note that some authors use Equation (6) but replace the symbol E with ε , ^{29,30} while other Also, while many authors represent the coupling factor with ρ , 33,39,40 some authors use the symbols ξ , $^{4,35,41-43}$, σ^{37} or k^{44} for the coupling factor with the same meaning as defined for ρ in Equation (5a). Other authors and much of the NOE community define $\sigma = w_2 - w_0$ and $\rho = w_0 + 2w_1$ $+ w_2$. ^{28,45,46} In the following discussions, we will use E and ρ as defined in Equations (5a) and (6) and translate literature values into E and ρ to provide consistency. Therefore, the numerical enhancement value found in a particular cited reference and the value given here might be different, due to the conversion between the different variables (e.g. E = A + 1).

2.2. DNP parameters

The coupling factor is the most relevant parameter for DNP, as it is the difference of the transitions that cause polarization enhancement (w_2 and w_0) relative to all nuclear spin transitions caused by relaxation through the electron spin. In the extreme narrowing limit ($\omega \tau_{\rm t} \to 0$), the upper limit of ρ is 0.5 if cross relaxation is of exclusively dipolar nature, and the lower limit of $\rho=-1$ is reached if scalar relaxation is the only pathway. As discussed below, the coupling factor sensitively depends on the time-scale modulating the electron–nuclear spin interaction at a given magnetic field and thus is related to molecular diffusion and the distance between the two spins. This provides the opportunity to measure molecular dynamics and structure through DNP (and NOE), and thus makes the determination of the coupling factor an important experimental goal.

The leakage factor f quantifies the fraction of nuclear spin relaxation caused from coupling to the electron spin, as it is defined as the ratio of the sum of dipolar and scalar transitions over all possible nuclear relaxation pathways. A leakage factor of f=1 means that all nuclear spin relaxation is caused by coupling to the electron, while f=0 shows that no nuclear relaxation is caused by the electron spin. The leakage factor is easy to experimentally determine by measuring the longitudinal relaxation time of the sample with radicals (T_1) and without radicals (T_{10}) and using the relation

$$f = 1 - \frac{T_1}{T_{10}}. (7)$$

The leakage factor depends on radical concentration through T_1 . Assuming that the electron spin concentration is dilute relative to the nuclei, Equation (7) can be rewritten as

$$f = \frac{kCT_{10}}{1 + kCT_{10}} \tag{8}$$

where k is the relaxivity constant of the radical species and C is the concentration of the radicals.

The saturation factor gives the degree to which the applied radio-frequency (RF) field saturates the electron transition of all radicals in the sample and can range from 0 to 1. The saturation factor can be written as a function of the applied radiation power P,

$$s = \frac{\alpha P}{1 + \alpha P} \tag{9}$$

where α is a constant related to the electron spin longitudinal and transverse relaxation times, T_{1e} and T_{2e} , as well as the properties of the ESR coil or cavity that is used to excite the sample.⁴

From here, the saturation factor requires further discussion. Equation (9) is correct for radicals with a single ESR transition; however, the picture becomes more complicated for radicals with more than one transition due to hyperfine splitting. The nitroxide radicals commonly used for ESR and DNP fall into this category, 47,48 as the unpaired electron in these molecules partially resides on a nitrogen nucleus with spin 1 (14 N) or spin 1/2 (15 N) giving three or two hyperfine lines, respectively. For the more common 14 N nitroxide radicals, at low concentrations in aqueous solutions the right side of Equation (9) is multiplied by a factor of 1/3, as only one hyperfine line can be saturated at a time. However, two processes can serve to mix the hyperfine lines and increase the saturation factor in the limit of infinite power (s_{max}) of nitroxide radicals well beyond $s_{max} = 1/3$.

For systems where molecular collisions between radicals occur rapidly compared to T_{1e} , Heisenberg electron spin exchange will mix the hyperfine lines. This is a process where two colliding radicals with opposite electron spin states exchange their electron spins, and if the nitrogen nuclei on the two radicals are in different spin states then the hyperfine lines are mixed as a result. Through efficient electron spin exchange, the maximum possible saturation factor can reach $s_{\rm max}\approx 1$ at nitroxide radical concentrations in water from tens of millimolars up to 100 mM concentrations, as reported by Armstrong and Han and Franck et al. 50,51 A recent report by Höfer et al. gives another demonstration of electron

spin exchange, as the authors investigated the concurrent saturation of both ESR lines of ¹⁵N, ¹⁶D-4-oxo-TEMPO (where TEMPO is the nitroxide radical most commonly used for DNP, 2,2,6,6-tetramethylpiperidine-1-oxyl) and noticed no difference in the DNP-amplified signal between saturating a single line and saturating both hyperfine lines.

Another process that can mix nitroxide hyperfine lines is fast nitrogen nuclear spin relaxation, 50 which can be extremely efficient when the rotational mobility of the nitroxide radical is restricted. 52 If the relaxation of the nitrogen nucleus is faster than that of the nitroxide's electron spin, the electron 'sees' more nitrogen spin states while being irradiated, and thus the hyperfine lines are mixed (i.e. all hyperfine lines can be effectively saturated) while irradiating only one of the hyperfine resonances. Because nitrogen nuclear spin relaxation begins to affect DNP when nitroxide motion is restricted, 52 nitroxides tethered to solid matrices, macromolecules, proteins or even unstructured proteins and smaller peptide oligomers can easily reach $s_{\rm max}=1$, even though adjacent radicals do not frequently come close enough to undergo collision-driven Heisenberg spin exchange. This has been experimentally demonstrated by observations that immobilized 14 N and 15 N nitroxide radicals give the same enhancement in the limit of infinite power, even with different numbers of hyperfine lines. 53

These descriptions of the saturation factor are based solely on classical T_1 relaxation dynamics of the electron populations and do not include electron–nitrogen spin–spin (T_2) relaxation effects due to spin coherences. To include electron–nitrogen T_2 effects into the saturation factor, semiclassical relaxation theory^{25,54} can be used, and a recent paper by Sezer et al. presents a formalism to include these effects. ⁵⁵

The isolation of the coupling factor is very important to gaining the desired information from an experiment. The first step towards isolating the coupling factor is to measure signal enhancement as a function of ESR saturation power and extrapolate to infinite power. This determines the maximum enhancement, E_{max} , where

$$E_{\text{max}} = 1 - \rho f s_{\text{max}} \frac{|\gamma_{S}|}{\gamma_{I}}.$$
 (10)

Since the leakage factor can be easily calculated from T_1 relaxation data, and γ_S/γ_I is constant, that only leaves the determination of $s_{\rm max}$ before the coupling factor can be directly accessed. For solutions of radicals where Heisenberg exchange is prominent, $E_{\rm max}$ must be measured as a function of concentration and extrapolated to infinite concentration where $s_{\rm max}=1.^{26,50}$ For immobilized or tethered radicals, nitrogen nuclear spin relaxation effectively mixes the hyperfine states in virtually all cases (small peptides may be an exception) and $s_{\rm max}\approx 1$ can safely be assumed. ^{53,56} Alternately, the determination of $s_{\rm max}$ can be avoided

entirely, and instead NMR T_1 relaxation dispersion (NMRD) is used to extract the coupling factors; this approach is discussed in Section 3.1.

It should be noted that additional considerations need to be made when working with nuclei other than hydrogen. First, while ¹H nuclei display almost exclusively dipolar coupling to electron spins, 21,26,57,58 other nuclei (such as ¹³C) can show pure dipolar enhancement or a mix of scalar and dipolar effects, depending on the molecule. 24,58-60 For carbon, scalar coupling is often observed for ¹³C atoms close to the large electron cloud of a halogen atom 46,58,60 or for systems where the radical and nuclei are held in close contact, 24,27 as scalar coupling requires an overlap of the electron and nuclear wavefunctions to be effective (from the $|\psi(0)|^2$ term in Equation (2a)). Also, for DNP with nuclei other than hydrogen, the three-spin effect needs to be considered. First described by Hausser and Reinbold in 1962,⁶¹ the three-spin effect describes DNP in a system with a radical and two nuclear spins that are coupled to each other. Using ¹³C and ¹H as an example, the ¹³C can be enhanced either through direct contact from the radical or through the NOE from nearby protons that have also been hyperpolarized by the radical. This leads to a modification of the enhancement equation (Equation (6)) to give

$$E_2 = 1 + \rho_2^S f_2^S s \frac{\gamma_S}{\gamma_{I_2}} + \rho_2^1 f_2^1 \frac{\gamma_{I_1}}{\gamma_{I_2}} (1 - E_1)$$
(11)

where the detected species (i.e. carbon) is nuclear spin 2 and third species (hydrogen) is nuclear spin 1. The symbol ρ_2^S indicates the coupling factor of spin 2 due to its interaction with the electron spin S (DNP), and ρ_2^1 is the coupling factor between carbon and hydrogen (NOE). Note that the negative sign of the electron's gyromagnetic ratio has not been factored out in Equation (11) as it was in Equation (6). A few papers in the recent literature have discussed the three-spin effect. 24,62,63

In an idealized scenario, the largest possible enhancement through Overhauser DNP can be found for the case of exclusive dipolar coupling by using Equation (6) with $\rho=0.5, f=1, s=1$ and the value of $|\gamma_S|/\gamma_I$ for the specific electron–nuclear spin pair (658 for 1 H, 2618 for 13 C and -6494 for 15 N, assuming g=2). This gives the largest enhancements of E=-328 for 1 H, E=-1308 for 13 C and E=3248 for 15 N. For the case of exclusively scalar coupling, $\rho=-1$ and the largest enhancements are E=659 for 1 H, E=2619 for 13 C and E=-6493 for 15 N.

2.3. Modelling the coupling factor

After the coupling factor has been determined, models of molecular interactions can be used to calculate the correlation time, τ_c , which describes the dynamics of the system. The process of calculating τ_c from

 ρ is simplified when the assumption can be made that coupling is dominated by dipolar interactions. While mixed scalar and dipolar models can be employed, previous studies have shown that ¹H DNP of nitroxide radicals dissolved in water is almost exclusively dipolar, ^{21,57,58} thus making this a fair assumption since most recent Overhauser DNP experiments in liquids utilize nitroxides and water molecules. In addition, it is assumed that the electron spin relaxation time constants T_{1e} and T_{2e} are much greater than τ_c , which is the case for nitroxide radicals where T_{1e} and T_{2e} are typically tens to hundreds of nanoseconds, while τ_c is usually tens to hundreds of picoseconds. This allows us to use a single spectral density function $j(\omega, \tau_c)$ to describe the coupling factor as

$$\rho = \frac{6j(\omega_S + \omega_I, \tau_c) - j(\omega_S - \omega_I, \tau_c)}{6j(\omega_S + \omega_I, \tau_c) + 3j(\omega_I, \tau_c) + j(\omega_S - \omega_I, \tau_c)}$$
(12)

where ω_S and ω_I are the electron and nuclear Larmor frequencies, respectively. Selecting or developing the suitable spectral density function assuming a suitable dynamic model is the first step of extracting dynamics information from the coupling factor.

For systems where translational motion best describes the dynamics at timescales relevant to DNP, a number of different spectral density functions have been used to investigate the coupling factor. 4,26,41,64 Here, we describe the force-free hard sphere (FFHS) model developed by Hwang and Freed because it has been widely used in recent work, 26,41,67 and there are no other obvious models for obtaining an analytical expression for the spectral density function that have clear benefits over the FFHS model while providing similar versatility. The FFHS model describes translational Brownian diffusion where the spins are centered on hard spheres (whose excluded volume can be taken into account) with no forces acting between them. If we assume that the overall correlation time is the translational correlation time, $\tau_{\rm c}=\tau_{\rm t}$, and again assume that $T_{\rm 1e}$ and $T_{\rm 2e}$ are much greater than $\tau_{\rm t}$, a single reduced spectral density function can be written for all dipolar transition rates 65 :

$$\begin{split} j(\omega,\tau_{t}) &= \\ \frac{1 + \left(5\sqrt{2}/8\right)\left(\omega\tau_{t}\right)^{1/2} + \left(\omega\tau_{t}/4\right)}{1 + \left(2\omega\tau_{t}\right)^{1/2} + \omega\tau_{t} + \left(\sqrt{2}/3\right)\left(\omega\tau_{t}\right)^{3/2} + \left(16/81\right)\left(\omega\tau_{t}\right)^{2} + \left(4\sqrt{2}/81\right)\left(\omega\tau_{t}\right)^{5/2} + \left(\left(\omega\tau_{t}\right)^{3}/81\right)}. \end{split} \tag{13}$$

Equations (12) and (13) give a link between the coupling factor measured from a DNP experiment and the translational correlation time τ_t . This relationship is shown by the solid line in Figure 3, where the coupling factor is plotted as a function of the product of the electron Larmor frequency and the translational correlation time.

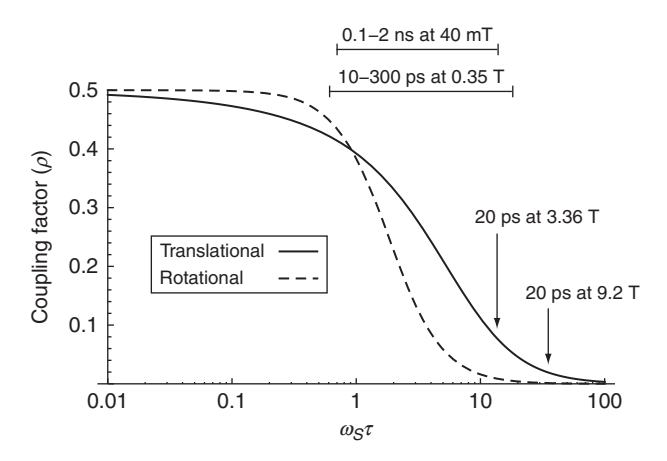


Figure 3 Plot of the coupling factor as a function of the electron Larmor frequency $\omega_{\rm S}$ times the translational correlation time $\tau_{\rm t}$ using the spectral density functions of Equations (13) and (15). Marked on the graph are regions or points pertaining to recently published reports. Experiments concerning changes in DNP for different systems are most effective where the small changes in correlation times will give appreciable changes in the coupling factor, and these regions are marked for 40 mT⁶⁸ and 0.35 T. 67,69,70 Experiments at higher magnetic fields have been more concerned with the amount of enhancement possible at these fields, and the correlation time given by the authors for nitroxide radicals dissolved in water is indicated at 3.36 41,71 and 9.2 T. 72

The translational correlation time can also be related to the molecular diffusion coefficients through the relation⁶⁵

$$\tau_{\rm t} = \frac{d^2}{D_I + D_S} \tag{14}$$

where d is the distance of closest approach between the radical and nuclei, and D_I and D_S are the diffusion coefficients of the nuclei and radical, respectively. Equation (14) is important because for systems where translational motion can be assumed, the results of a DNP experiment can give the values for the local diffusion coefficient of the two molecules at the point of interaction if the distance of closest approach is known, or at a given distance of closest approach. Separate experiments have shown that, for nitroxide radicals dissolved in water, the dynamics can be safely described using only translational motion. After d is calibrated through calculations or a reference experiment, the local diffusion coefficient of water interacting with a bound radical spin label can be found at the determined distance of closest approach d. Here, it is important to note that recent experiments show minimal differences in the coupling factors, and thus the distances of closest approaches, of chemically

different nitroxide radicals.⁷³ This process has recently been used to estimate local diffusion of water within $\sim\!10$ Å of the nitroxide radical on the surface of lipid vesicles,⁶⁷ inside polyelectrolyte coacervates⁶⁹ and on the surface of proteins.⁵⁶

Some systems cannot be well described by translational motion, so instead they require a model based on rotational diffusion. The commonly used model is one where the nuclei and radical form a bound complex, then this complex rotates to modulate dipolar coupling. ⁷⁴ Here, the overall correlation time consists of the rotational correlation time of the solvent complex, $\tau_{\rm r}$, and the exchange rate of molecules in and out of the complex, $\tau_{\rm m}$, where $1/\tau_{\rm c}=1/\tau_{\rm r}+1/\tau_{\rm m}$. The form of this spectral density function is simpler ^{4,25}:

$$j(\omega, \tau_{\rm c}) = \frac{\tau_{\rm c}}{1 + \omega^2 \tau_{\rm c}^2} \tag{15}$$

Although the lifetime of the bound complex needs to be accounted for, it is often the case that $\tau_r\gg\tau_m$ so that τ_m can be ignored. A plot of the coupling factor versus magnetic field and the rotational correlation time is given by the dashed line in Figure 3.

These same models are also used to interpret NMRD measurements. NMRD is the measurement of relaxation rates $1/T_1$ as a function of magnetic field, and the data from such an experiment can be fit to a model to extract the coupling factor. A26,41 Both DNP and NMRD can, in principle, give access to the same coupling factor and correlation times. DNP can directly measure the coupling factor without employing a model for molecular dynamics (and the spectral density function) if the saturation and leakage factors are known or can be determined (through Equation (10)), but a model is required to calculate the correlation times from ρ (Equations (12) and (13)). NMRD data provide both the coupling factor and correlation times, but the determination of either quantity requires the use of an appropriate model. A more complete description of the models used for NMRD can be found in the literature. A26,744–78

While these models match experimental data reasonably well at lower fields, recent experiments at higher magnetic fields of 3.4 and 9.2 T show enhancement values that are much higher than predicted with the currently employed theory. At these higher fields, the timescale of molecular interactions that give rise to Overhauser DNP effects is much shorter (sub-picoseconds to picoseconds) and thus should be more sensitive to the rotational diffusion dynamics of water, closely related to the atomistic details of the radical and solvent, instead of translational diffusion dynamics. These atomistic details are not accurately represented in the FFHS or rotational models (Equations (13) and (15)), implying that further work needs to be done to develop more accurate models.

Due to the imperfections of the FFHS and other models at high magnetic fields, molecular dynamics (MD) simulations have recently been proposed to calculate the coupling factor,³⁵ eliminating the need for explicitly translational or rotational models in an ideal scenario. In this approach, the MD simulations are used to calculate correlation functions for the electron–nuclear dynamics. The correlation functions are then related to the computed spectral density functions that are connected to the coupling factor as discussed above. While the first efforts in this direction show promising results that come closer to explaining experimental results at high magnetic fields, further development of theory and computational approaches is needed for MD simulations to become a reliable and generally usable tool for computing the coupling factor.

3. EXPERIMENTAL RESULTS

The details, outlook and potential of a DNP experiment depend on the choice of the external magnetic field, through the dependence of the electron Larmor frequency on field. The hardware required for the experiment varies dramatically between the different frequencies and field regimes. Also, the type of studies that are feasible vary with field as well, due to the quality of the thermally polarized signal, the maximum sample size for the different ESR frequencies and the accessible dynamic timescales. Most importantly, the coupling factor decreases with increasing field leading to further restrictions on the systems available for study at different field strengths. Therefore, this section is divided into parts dedicated to the different field regimes used for DNP studies.

3.1. Measuring the coupling factor

Before investigating each individual field regime, it is illustrative to discuss recent attempts to accurately measure the coupling factor. A DNP experiment can measure $E_{\rm max}$ (by extrapolating enhancement values to infinite power), but $E_{\rm max}$ is related to the product of ρ , f, $s_{\rm max}$ and γ_S/γ_I , as shown in Equation (10). As f can be measured separately and γ_S/γ_I is a constant, determining the coupling factor ρ from maximum enhancement measurements only requires separating the coupling factor from the maximum saturation factor $s_{\rm max}$. For radicals with a single hyperfine line, $s_{\rm max}=1$ and the coupling factor is easy to determine. For nitroxide radicals with two or three hyperfine lines, the determination of $s_{\rm max}$ values needs further careful consideration. 26,50,71

Many authors have published reports comparing the DNP performance of different radicals but have in the past given conflicting or occasionally unphysical values for the coupling factor. Grucker et al.

measured DNP performance and calculated the coupling factor of multiple nitroxide radicals in buffer solutions with 1 mM nitroxide radical concentrations, but assumed that $s_{\rm max}=1/3$ at 6.85 mT.³⁷ Benial et al. also assumed that $s_{\rm max}=1/3$ for ¹⁴N nitroxides and $s_{\rm max}=1/2$ for ¹⁵N nitroxides between 0.45 and 5 mM and measured coupling factors at \sim 6 mT of 0.45 and 0.46 for ¹⁴N and ¹⁵N nitroxides, respectively.³⁹ Nicholson et al. measured the DNP of 4-oxo-TEMPO with the assumption that 1/n, where n is the number of hyperfine lines of the sample.⁴⁹ The authors assumed that n must be greater than 3 due to the additional ESR transitions that become allowed at low magnetic fields, and this assumption was required to explain their data which would give a coupling factor of larger than 0.5 at 10 mT if n=3.

In 1977, Bates and Drozdoski showed that Heisenberg electron spin exchange would affect DNP enhancements by increasing s_{max} with increasing radical concentrations from $s_{\text{max}} = 1/3$ to a limit of $s_{\text{max}} \approx 1.^{31}$ Recent experiments have shown that, indeed, electron spin exchange critically affects DNP experiments with radical concentrations above 0.5 mM,⁵⁰ thus encompassing the bulk of commonly performed DNP experiments. Despite this, Bates and Drozdoski's work went unnoticed by much of the DNP community except for a few authors who mentioned electron spin exchange in their DNP papers but did not take the step of calculating coupling factors with this consideration. 62,82,83 Armstrong and Han revived the discussion of the coupling and saturation factors in the literature on the coupling factor by using Heisenberg electron spin exchange to describe their DNP enhancement data from nitroxide radicals in water. 50 This renewed the focus on electron spin exchange, as demonstrated by Armstrong et al.²⁶ and Garcia et al.,⁶⁸ where coupling factors were calculated by measuring E_{max} as a function of concentration and extrapolating to infinite concentration. At infinite concentration, it can be assumed that $s_{max} = 1$ (experimentally achievable high nitroxide concentrations on the order of ~ 100 mM closely approach this limit⁵¹), allowing for the measurement of coupling factors. In a separate paper, Armstrong et al. used this method to calculate the coupling factors of pyrroline and piperidine ring radicals (five- and six-membered rings, respectively) and compared these results with MD simulations of several key parameters for these two radicals, finding that there were no differences in any of the parameters that affect DNP. 73 This allows for the accurate comparison of DNP results between the pyrroline rings, commonly used to label proteins, and piperidine ring radicals, commonly used in small molecule DNP work.

A recent advance in the quantification of DNP came with the inclusion of nitrogen nuclear relaxation into the saturation factor. Inspired by the measurement of nitrogen spin–lattice relaxation times over a wide range of correlation times by Robinson et al., ⁵² Armstrong and Han developed a

formalism to allow for the mixing of nitroxide radical hyperfine states by taking both Heisenberg electron spin exchange and nitrogen nuclear relaxation into account. This included an explicit formula for s_{max} in terms of the electron spin exchange rate, electron spin relaxation rate and nitrogen nuclear spin relaxation rate. An interesting outcome of this model is that $s_{max} \approx 1$ for nitroxides with slow motion/long correlation times, such as spin labels bound to larger molecules (including peptide oligomers or disordered proteins with high protein mobility⁵⁶) or immobilized to solid supports. This was shown experimentally with immobilized ^{14}N and ^{15}N nitroxide radicals that had nearly identical $E_{\rm max}$ values,53 and with spin-labelled tau proteins that only provided reasonable $E_{\rm max}$ values when $s_{\rm max} \approx 1$ is assumed.⁵⁶ The tau proteins also gave E_{max} values that did not change when the freely dissolved proteins aggregated to form immobilized fibres that significantly broadened the ESR spectrum of the spin label, indicating that the monomeric (freely dissolved) tau protein's mobility is already sufficiently hindering the nitroxide radical motion to fulfil the condition of $s_{\text{max}} \approx 1$.

Other authors, when faced with the determination of $s_{\rm max}$ before calculating a coupling factor, have opted to not calculate a coupling factor from DNP data, but instead use NMRD on the same system to compute the coupling factor. As mentioned above, NMRD data can be fit to give a coupling factor by using the same models and spectral density functions used for DNP (i.e. Equations (12) and (13)). This method was initially proposed by Hausser and Stehlik⁴ and first demonstrated by Höfer et al., ^{29,41,77} where the NMRD curves for 4-hydroxy-TEMPO are fit to provide a correlation time of $\tau=15$ –20 ps. This correlation time gave a coupling factor of $\rho=0.36$ at 0.34 T and $\rho=0.06$ at 3.36 T, which was compared to the observed DNP enhancements of E=-100 and E=-20 at 0.34 and 3.36 T, respectively.

Shortly after the study by Höfer et al., Armstrong and Han demonstrated that the maximum saturation factor can be experimentally determined directly through DNP experiments, achieving good agreement between theoretical and experimental $s_{\rm max}$ values for 4-oxo-TEMPO. The coupling factor can then be determined with the calculated value of $s_{\rm max}$ by measuring $E_{\rm max}$ as a function of radical concentration then extrapolating to infinite concentration. The coupling factor of $\rho=0.22$ determined in this manner gave a translational correlation time of $\tau=76$ ps, which is higher than the NMRD value. Armstrong and Han confirmed the previous NMRD finding through independent relaxation measurements carried out in collaboration with S. Stapf and C. Mattea, showing that there is indeed a disagreement between DNP and NMRD calculations of the coupling factor and dynamics on the example 4-oxo-TEMPO, where the NMRD fit values gave $\tau=24$ ps and $\rho=0.36$ at 0.35 T. The authors suggested in 2009 that the disagreement in the methods is due to the

limitations of the available models for describing the spin dynamics interactions. However, more recent measurements by Türke et al. ⁷¹ and Franck et al. ⁵¹ show that the coupling factor determined through DNP measurements can approach higher values, much closer to the NMRD values of $\rho \approx 0.30$ –0.35, depending on the choice of instrumental and experimental conditions (such as sample heating and the quality factor of the microwave resonator). This conclusion is contrary to the previous finding by Armstrong et al. of $\rho = 0.22$, ²⁶ and a discussion of this discrepancy is forthcoming. ⁵¹

To reach this conclusion, Türke et al. investigated the experimental parameters that should affect the evaluation of DNP enhancement and found a condition where they believed complete saturation of the ESR line occurred with no sample heating for ¹⁵N, ¹⁶D-4-oxo-TEMPO. ⁷¹ From there, they measured actual enhancements of E = -170 at 0.35 T, yielding a coupling factor of $\rho \leq 0.34$ at 27 °C. This experimental DNP data more closely approaches the NMRD data in the accompanying paper by Bennati et al., where a coupling factor of $\rho = 0.35$ was determined at 25 °C, which corresponds to a maximum predicted DNP signal enhancement of $E_{\text{max}} = -218.^{76}$ Electron–electron double resonance (ELDOR) experiments led the authors to assume $s_{\text{max}} = 0.8$ for the given sample and instrumental setting, in which case, the actual enhancement E from the DNP experiments and E_{max} from NMRD are in good agreement. The authors did not present DNP measurements as function of power, instead stating that they had achieved maximum saturation in a single measurement.

The Han group's most recent experimental results, 51 however, show that extrapolation to infinite power can lead to higher s_{max} and E_{max} values, thus experimentally achieving the limit predicted by NMRD data ($\rho = 0.36$ at 0.35 T) with DNP measurements. While the values of the coupling factor previously published by the Han group will need revisiting, their prior key conclusions, that one can operate under experimental conditions where $s_{\text{max}} \approx 1$ and that the coupling factors can be obtained with this model-free approach using optimized instrumental settings, are still valid. This is especially true now that the previous discrepancies between different research groups and between NMRD and DNP data have been resolved. This conclusion has significant implications because Overhauser DNP is inherently much more sensitive than NMRD measurements as it relies on large signal enhancements rather than signal decay, and also because time-resolved hydration dynamics measurements are potentially viable with Overhauser DNP but not with NMRD methods. Although corrections to previously published absolute ρ values need to be made, note that relative ρ values, and thus changes in correlation times (τ) , measured with the same instrumental and experimental settings remain correct. Therefore, for example, the findings by Kausik et al.,⁶⁷ Pavlova et al.⁵⁶ and Ortony et al.⁸⁴ that the translational diffusion of hydration water on a given protein, macromolecule or lipid vesicle surface is two- to four-fold slower compared to bulk water is still valid.

Besides Overhauser DNP and NMRD, a third method to determine the saturation and coupling factor that relies on MD simulations has been demonstrated by Sezer et al. 35,55 As mentioned previously, MD simulations are used to calculate correlation functions for the electron-nuclear interactions, which were used to compute spectral density functions, yielding a coupling factor of around 0.3 at 0.35 T. This number is slightly lower than the values determined from DNP and NMRD, but still in reasonable agreement. To calculate the saturation factor, the effects of electron–nuclear spin–spin (T_2) relaxation effects due to spin coherences were included with semiclassical relaxation theory^{25,54}. The saturation factor was combined with the previously calculated coupling factor to produce enhancement values, which compared well with experimentally determined values at 9.2 T. It should be mentioned that this treatment of the saturation factor by Sezer et al. included the effects of rapid mixing of the nitroxide's hyperfine states through fast nitrogen nuclear spin relaxation, and showed that these effects do increase the saturation factor, as predicted by Armstrong and Han.⁵⁰ However, this effect is small for the particular example of nitroxide radicals freely dissolved in solution, unlike the case of tethered nitroxide labels.

As the discussion in this section shows, there remains somewhat conflicting reports on the proper way to measure the coupling factor and maximum saturation factor for nitroxide radicals. While this is not a concern for radicals (such as trityl) with only one hyperfine line, nitroxide radicals have been shown to give generally better DNP signal enhancements for solution-state systems than water-soluble trityl radicals at both 0.34 and 3.3 T.⁴¹ Because of the importance of nitroxide radicals, further work needs to be done to resolve all discrepancies. However, the most recent results show that theory and various experimental reports are closer in agreement than ever before.

3.2. Low magnetic fields: Below 0.1 T

DNP at very low magnetic fields is attractive for two reasons. First, the electron saturation frequency at low fields is in the radiofrequency range, where it is much easier to obtain high-power radiation sources, amplifiers and transmission equipment. In fact, the first experimental verifications of the Overhauser effect were conducted between 1 and 5 mT, ^{2,85,86} likely due to the ease of constructing a suitable magnet and equipment to perform ESR saturation. The second reason for adding DNP to a low-field system is to help overcome the limited thermal polarization at low

fields, which is especially important for portable NMR applications using simple magnet designs or the earth's magnetic field.

One consideration that needs to be made for low-field DNP studies is the unique behavior of nitroxide radicals at very low magnetic fields, affecting the optimal frequency for ESR saturation. At fields of $\sim\!0.1$ T and higher, the electron spin and nitroxide nitrogen spin are coupled only through the hyperfine interaction, leading to the familiar three ESR transitions for ^{14}N nitroxides or two ESR transitions for ^{15}N nitroxides. However, at lower fields, the electron and nitrogen spins are strongly coupled, leading to unequal intensities and spacing of the hyperfine lines below 0.1 T and additional allowed transitions that become significant below 3 mT. To visualize this effect, Figure 4 shows the simulated DNP-detected ESR spectrum at X-band (0.35 T) and a low field value of 1.5 mT (chosen because of recent studies at 1.5 mT 32,87,89). The detailed theory of DNP with nitroxides in low fields has been thoroughly described by other authors, $^{36,87,88,90-94}$ so it will not be reproduced here.

The beauty of low-field DNP is the simple and versatile hardware that can be employed for experiments. Magnetic fields under 40 mT are experimentally easy to generate with electromagnets, ^{87,88,95,96} permanent magnets, ⁶⁸ the fringe field of a superconducting magnet ⁹⁷ or even the earth's magnetic field. ⁹⁸ Any number of coil designs can be used for ESR saturation and NMR detection, depending on the frequencies required. Usually two separate coils are used ^{36,87,99}; however, a special double-resonant single-coil probe was designed and demonstrated at 2.7 mT by TonThat et al. ⁹⁵ The radiofrequency electronics are also much easier to acquire and build than those needed for higher frequencies. An example of a recently described experimental system for DNP at 1.5 mT is shown in Figure 5.

Many reports of low-field DNP are focused on expanding the knowledge base of the type and magnitude of signal enhancements observed in

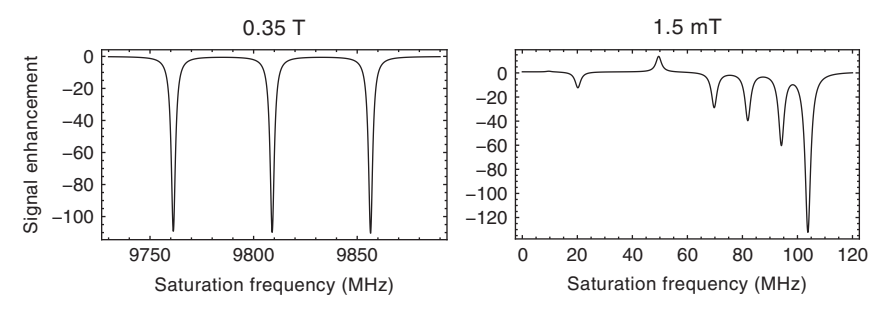


Figure 4 Plots of the DNP-detected ESR spectra of a ¹⁴N nitroxide radical at 0.35 T and 1.5 mT. The low-field spectra includes both π and σ transitions. The reader is referred to the literature for further details. ^{32,36,87,88}

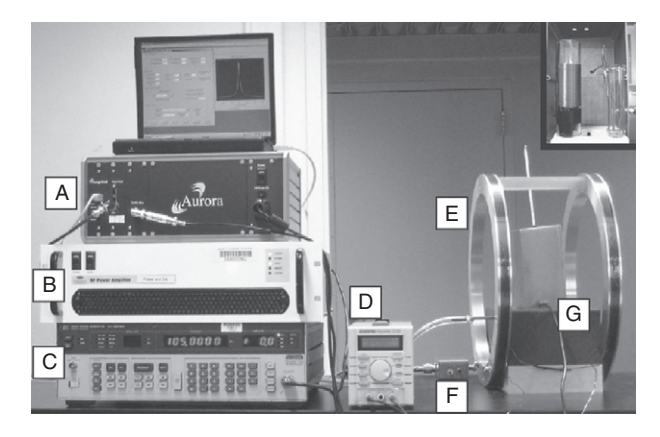


Figure 5 Photograph of a recently published 1.5 mT DNP–NMR system. Labelled in the photograph are the (A) NMR spectrometer, (B) ESR saturation amplifier, (C) signal generator for ESR saturation, (D) magnet power supply, (E) electromagnet, (F) home-built LC tuning circuit and (G) sample RF shielding box. The inset in the upper right shows the inside of the RF shielding box, with the NMR coil on the left and a birdcage coil for ESR saturation on the right. During operation, the ESR coil is placed coaxially inside the NMR coil. Adapted with permission from Ref. [87].

different chemical systems. Sapunov and Chirkov investigated an aromatic nitroxide radical (4,4'-di(tert-butyldiphenyl)-N-oxyl) in hexane, decane and dimethylformamide (DMF) at 1.17 mT. 100 They found that the DNP interaction is mostly dipolar, and also determined electron spin exchange rate constants. Tregubenkov and Baldin derived analytical expressions for the 15N nitroxide radical at fields comparable to the hyperfine interaction and then recorded a DNP-detected ESR spectrum at 1.8 mT. 101 In addition to presenting the seminal formulation of lowfield DNP theory, Guiberteau and Grucker reported field-cycled DNP data to support their theory with NMR detection at 6.8 mT and ESR saturation between 4.5–9⁸⁸ and 0–4 mT.³⁶ Polyon et al. gave a larger set of field-cycled DNP data for both ¹⁴N and ¹⁵N nitroxides with ESR saturation from 0 to 8 mT and NMR detection at 59 mT. 93 Interestingly, TonThat et al. showed the only recent example of solution-state DNP experiments where the electron spin source is provided by a dissolved paramagnetic ion (MnCl₂/H₂O) in their paper that was aimed solely towards demonstrating a new double-resonant single-coil probe design. 95

A few papers have dealt with the effects of Heisenberg electron spin exchange on low-field DNP behavior. Bates and Drozdoski's initial description of spin exchange effects on DNP was tested against data collected at 7 mT,³¹ and further work by Bates showed the changes in the DNP-detected ESR spectra at 5–9.5 mT as radical concentration was increased.⁹² Tregubenkov et al. presented the calculated effects of spin

exchange on DNP at low fields, but did not provide any experimental data. ¹⁰² The most recent work on spin exchange in low-field DNP was published by Lingwood et al. using an addition to Guiberteau and Grucker's theory to allow for spin exchange at 1.5 mT, where additional allowed nitroxide transitions lead to more than three ESR hyperfine lines. ⁸⁷

While low-field imaging experiments are discussed in Section 3.6, some reports have been published on low-field DNP spectroscopy with the aim of benefiting PEDRI experiments. The first is by Lurie et al., where they described the theory of field-cycled DNP in low magnetic fields and showed experimental results to help advance their ongoing imaging experiments with ESR saturation at 0.1-12 mT and NMR detection at 10 mT. 99 A similar study investigated the potential of DNP using pulsed electron saturation to reduce heating in large biological samples, with both ESR saturation and NMR detection occurring at 10 mT. ¹⁰³ In another experiment, Grucker et al. measured the DNP signal enhancement at 6.85 mT using 18 different nitroxide radical species in sodium phosphate buffer solutions, and also investigated the DNP efficiency of many of these radicals in albumin solutions, serum, red blood cell suspensions and whole blood with the aim of developing radicals for in vivo DNP applications.³⁷ The largest measured enhancement was $E_{\text{max}} = -40.6$ for 1 mM 2,2,4,4-tetramethyloxazolidine-N-oxyl dissolved in sodium phosphate buffer. In a similar study, Ardenkjær-Larsen et al. demonstrated the ESR and DNP properties of three different trityl radicals dissolved in water, saline, plasma and blood at 9.5 mT, obtaining DNP enhancements of up to $E_{\text{max}} = -277$ (at extrapolated infinite concentration, which corresponds to $\rho = 0.42$) with deuterated hydroxyl trityl dissolved in water. 64 Their experiments were aimed towards identifying optimal radical species for in vivo DNP and PEDRI studies. In addition to DNP experiments, the authors used NMRD to measure the correlation times of their samples, obtaining $\tau = 166$ ps for their system that gave the highest DNP enhancement. This correlation time for trityl radicals is much higher than the $\tau = 15-25$ ps that is measured with NMRD for nitroxide radicals, likely due to the larger distance of closest approach between the water molecules and the unpaired electron on the trityl radical. This provides further evidence that while the single ESR transitions of trityl radicals are easier to saturate, nitroxide radicals are generally a better agent for DNP due to lower correlation times (and shorter distances of closest approach, *d*) and thus yield larger coupling factors.

Another interesting application motivated by medicine is the use of the three-spin effect to determine lithium concentration solely through ¹H DNP measurements. In a proof of principle study by Zeghib et al., an increased concentration of ⁷LiOH in aqueous solution with trityl radicals resulted in a decreased ¹H DNP enhancement at 6.8 mT due to a competing three-spin effect. ⁹⁶ This was proposed to allow lithium monitoring

in vivo. However, the method suffers from the requirement for concentrations of lithium far exceeding biological values, as lithium concentrations of $0.5-2\,\mathrm{M}$ were measured in the study while the greatest biological values do not exceed 2 mM.

The simpler equipment design of low-field DNP systems has allowed researchers to move beyond developing the technique to investigating various chemical systems. A team at Hacettepe University built a 1.5-mT DNP system and performed multiple investigations on the low-field DNP properties of nitroxide radicals in various solvents and mixtures of solvents. Nitroxide radicals have been measured in methanol, 104 ethanol, tetrahydrofuran (THF) and dimethyl sulphoxide (DMSO) and in soybean oil mixtures. 106 DNP enhancement through both π and σ transitions was measured with nitroxides in water and phosphate buffer. Their most recent study recorded DNP and DNP-detected ESR spectra as a function of viscosity of water/glycerol solutions using 4-hydroxy-TEMPO, confirming that increased viscosity resulted in decreased signal enhancement due to the restriction of the translational motion of the molecules. 83

Researchers at Uludağ University also have published DNP studies at 1.5 mT,¹⁰⁷ focusing on chemicals extracted from asphalt and highly fluorinated solutions. The chemical from asphalt, asphaltene, intrinsically contains unpaired electrons which can be used for DNP analysis, and the study by Cimenoğlu measured DNP enhancement of asphaltene suspended in numerous solvents. 108 In this report, dipolar enhancement was observed for hydrocarbon solvents, and the enhancement values increased with the addition of CS2 to the mixture, due to the action of CS₂ to disperse asphaltene micelles and decrease the viscosity of the medium. The addition of CCl₄ had mixed effects depending on the other cosolvent in the mixture. Aydoğdu et al. also observed dipolar enhancement for asphaltene suspended in various xylene isomers. 109 Ersözlü et al. saw dipolar enhancement for asphaltene suspended in pure and mixed chlorobenzene and pyridine; the enhancement increased with chlorobenzene concentration and uniformly increased with temperature. 110 In a different study, Peksoz et al. tested the 19F DNP enhancement of the α , γ -bisdiphenylene- β -phenyl allyl (BDPA) radical in multiple fluorinated solvents and observed that the aliphatic solvents gave dipolar enhancement while the aromatic solvents gave scalar enhancement. 80 The scalar enhancement was interpreted as an effect of the delocalized electron in BDPA and stacking between the planar BDPA and the aromatic ¹⁹F solvent molecules creating electron spin density at the solvent nuclei. A follow-up study showed that when the BDPA radical was replaced with a galvinoxyl radical, the effect reversed somewhat due to the different radical structure: the aromatic solvents had large dipolar enhancements and the aliphatic solvents displayed a greater scalar character while still having a mostly positive coupling factor.⁸¹ A study by Ovalioğlu et al. investigated the ¹⁹F DNP-detected ESR spectra of galvinoxyl dissolved in *N*-methyl-bis-trifluoroacetamide (MBFA) and octafluorotoluene (OFT) and saw hyperfine structure in the MFBA spectrum that indicates a hyperfine interaction between the galvinoxyl radical and the nitrogen atom on the MFBA, indicating bond or complex formation between galvinoxyl radicals and MFBA.⁸⁹ In another study by the same authors, the ¹⁹F DNP-detected ESR spectra of BDPA in some highly fluorinated solvents were obtained, noticing that the intensity of the ESR peaks decreased at higher temperatures, while not discussing the dipolar or scalar nature of the enhancement.¹¹¹

Low-field DNP has also been used to study aqueous char suspensions at 11.7 mT in a series of papers by Odintsov, Clarkson and co-workers. After designing and testing the system with nitroxide radicals and the solvated electron of hexamethylphosphorous amide, 42 the initial report of ¹H DNP signal enhancement from the intrinsic free electrons contained in chars found that the hardwood char suspensions gave $E_{\text{max}} = +17.4$ and softwood char suspensions gave $E_{\text{max}} = -27.6$. The dominantly ¹H scalar enhancement of the hardwood chars was notable and was explained to be due to hydrogen bonding or chemisorption of the water onto the surface of the char followed by a slower molecular exchange process with the bulk water. The sign of enhancement for hardwood char suspensions was found to change with temperature, due to the delicate balance between the translationally mediated dipolar enhancement and the scalar enhancement/molecular exchange process; a plot showing this result is reproduced in Figure 6.34 The biological applications of this work were described in another paper, where imaging experiments were conducted that showed the feasibility of measuring dissolved oxygen concentration using aqueous char suspensions and PEDRI methods, owing to the changes in the ESR linewidth (and thus achievable ESR saturation) and leakage factor of the chars as the oxygen concentration varies. 113 Changing the oxygen concentration from 0% to 4% resulted in obvious differences in the PEDRI images with fructose chars. Finally, DNP enhancements of various char samples were compared to pulsed-field gradient (PFG) diffusion measurements of the water inside the porous structure of the chars, showing that the short-range nuclear-electronic interactions inside the pores have the dominant effect on DNP enhancements.114

DNP can also easily be performed in the earth's magnetic field. Halse and Callaghan recently demonstrated DNP with detection in the earth's field and hyperpolarization of the ¹H NMR signal of water with and without field cycling, using a modified commercial earth-field MRI system. ⁹⁸ Both methods of performing DNP gave enhanced magnetization greater than what would be feasibly possible with prepolarization in a

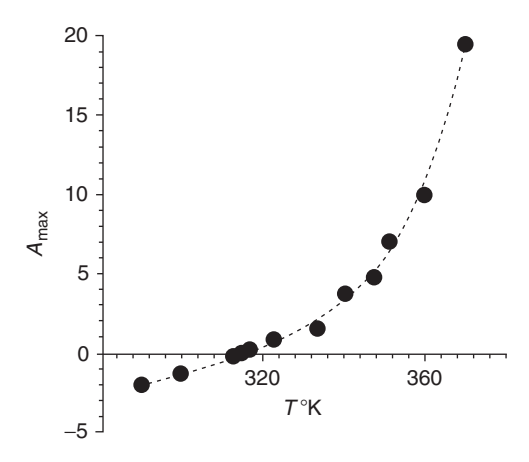


Figure 6 Temperature dependence of the DNP enhancement of water protons in an aqueous suspension of hardwood char. The dramatic change with temperature is due to the interplay between translational motion and the exchange rates of water tightly bound to the char. $A_{\text{max}} = E_{\text{max}} + 1$. Reproduced with permission from Ref. [34].

higher magnetic field. A 2D ¹⁹F⁻¹H correlation spectroscopy spectrum of 2,2,2-trifluoroethanol doped with TEMPO was presented as the motivation and outlook for 2D NMR techniques in the earth's magnetic field. In addition to spectroscopy, earth's field DNP can also be used to create new devices, such as a sensitive magnetometer using DNP to measure small changes in the earth's magnetic field.¹¹⁵

In the discussion of their 1.5 mT DNP system, Lingwood et al. ⁸⁷ compared the enhanced signal possible at 1.5 mT to that reported by Halse and Callaghan. ⁹⁸ The higher theoretical enhancement in the earth's magnetic field is outweighed by low thermal polarization, and the DNP-enhanced signal intensities are comparable in the earth's field and at 1.5 mT. However, the signal-to-noise ratio (SNR) of DNP-enhanced signal at 1.5 mT is expected to be 380 times larger than in the earth's field because the SNR of a magnetic resonance experiment increases with the proton detection frequency by an additional factor of $\omega_{\rm H}^{3/4}$, given equal polarization. ¹¹⁶ This shows that the SNR will be greater at low fields such as 1.5 mT than in the earth's magnetic field. However, the earth's field will be superior for some applications (such as 2D spectroscopy) due to the natural homogeneity of the earth's magnetic field, which is difficult to reproduce with a portable magnet system.

Garcia et al. describe the design of an L-band DNP spectrometer at 40 mT, employing an ESR frequency of 1.1 GHz, and report a coupling factor for 4-oxo-TEMPO dissolved in water of $\rho = 0.39.^{68}$ This coupling factor corresponds to a translational correlation time of $\tau = 150$ ps, which implies that the actual coupling factor at 40 mT should be higher to yield

correlation times similar to the $\tau=\sim\!20$ ps measured at 0.35 T for the dissolved nitroxide—water system. The discrepancy may come from the fact that the quality factor of the loop-gap resonator is low, so that ESR saturation close to $s_{\rm max}$ could not be achieved. This discussion shows that DNP instrumentation needs to be perfectly optimized and calibrated to provide absolute values for molecular dynamics. In any case, a key benefit of DNP at 40 mT is the sensitivity to changes in the molecular dynamics of systems with correlation times on the order of 0.1–10 ns, that is, longer timescales that are assessable at $\sim\!0.3$ T fields. Therefore, dynamics that are similar to or up to 10 times slower than bulk water (with $\tau_{\rm t}$ on the order of 20 ps) are more sensitively detected at 0.35 T, while the dynamics of significantly hindered or entrapped water, or even the structural water of proteins, can be more sensitively detected at 40 mT.

In addition, multiple researchers have used polarization at low magnetic fields strengths (10–54 mT) followed by flowing or shuttling the sample to higher fields (4.7–7 T). 97,117–121 Since these experiments involve changing magnetic field strengths, they are discussed in further detail in Section 3.5.

3.3. Magnetic fields corresponding to X-band ESR: 0.3-0.35 T

Moderate magnetic fields are well suited for solution-state DNP. Interestingly, the only published solution-state DNP experiments between 0.1 and 1 T have been performed at the magnetic fields corresponding to X-band ESR, due to the commercial availability of X-band ESR systems operating at 0.3–0.35 T. The higher field increases the detection sensitivity for both the unenhanced and enhanced signal, while the coupling factor at 0.35 T is in an ideal range for studying solution dynamics of the disordered and highly dynamic hydration water that solvates macromolecules, as the solution dynamics are typically by a factor of 2–10 slower than bulk water.

The equipment and hardware for X-band DNP experiments are more complex than at the lower fields discussed so far. The higher field strength of the magnet cannot be produced with simple solenoids; instead, complex superconducting magnets, electromagnets or permanent magnet arrays 122,123 must be used. Electron saturation frequencies are in the microwave region (8.4–9.8 GHz) and are more difficult to generate, amplify and transmit to the sample than radiofrequency signals. Coils cannot be used to achieve ESR saturation of the sample; instead, resonant cavity structures or horn antennas are required. However, these frequencies are still low enough that they will penetrate a small aqueous sample up to ~ 1 mm thickness. If a commercial X-band ESR system is used, NMR detection can be included through small radiofrequency NMR probes inserted into the microwave cavity or by use of an electron–nuclear double resonance (ENDOR) cavity with an added

home-built tuning circuit.²⁹ The output of the ESR system can be directly used for electron saturation,^{29,50} or higher power microwave sources can be installed.^{71,122} With some hardware modifications, these systems allow for concurrent ESR and DNP experiments, which have several practical advantages.

Much of the recent development of theory and methods for measuring the coupling factor has been performed with X-band DNP. 26,29,41,50,71,73 Since these studies were discussed earlier in Section 3.1, they are not included here and instead this section covers recent applications for DNP carried out at this field.

One of the main focuses of recent work at moderate fields has been the development of X-band DNP for the investigation of soft matter systems through the measurement of translational dynamics of hydration water interacting with molecular and material surfaces. The first work in this area involved the ¹H enhancement of water using spin-labelled fatty acids (the radical is bound to the fatty acid molecule). McCarney et al. showed that DNP enhancement of water is larger inside spin-labelled stearic acid micelles and smaller within vesicle bilayers assembled of spin-labelled stearic acid and stearate. 70,125,126 This is due to the different water accessibility of the fatty acid hydrocarbon tail within these structures, likely owing to different curvature and packing density of the assemblies. This result is reproduced in Figure 7. Kausik and Han extended this work to the quantification of local diffusion coefficients of water within 10 Å distances of the lipid vesicle surface, which encompasses up to approximately three water layers (also referred to as hydration water or outer sphere water).⁶⁷ They reproduced the findings of theory and quasi-elastic neutron scattering studies that the local diffusion coefficients of hydration water are impeded compared to bulk water diffusion by about two- to four-fold. This approach is unique in that local and interfacial information can be obtained in the complete presence of bulk water, and that such dilute concentrations (<1 mM) and small sample volumes ($<10 \mu l$) can be used. For these applications, the enhanced signal comes solely from the interaction of water with the spin label within molecular distances of up to ~ 10 Å. The fast exchange of water compared to the timescale of the 1 H T_1 relaxation leads to polarization build-up of the bulk water signal that is modulated only due to these local interactions. Overhauser DNP has also been used to investigate the local water dynamics of coacervating polyelectrolyte systems, where the diffusion coefficients of the water interacting with the spin-labelled polymers were found to decrease by an order of magnitude when the polyelectrolytes assemble into a dense liquid coacervate phase suspended in a dilute solvent phase. ⁶⁹ Dollman et al. synthesized thermoresponsive spin-labelled hydrogels which spontaneously collapsed as the temperature was increased, with the intent to polarize molecules inside the gel matrix and subsequently expel the polarized

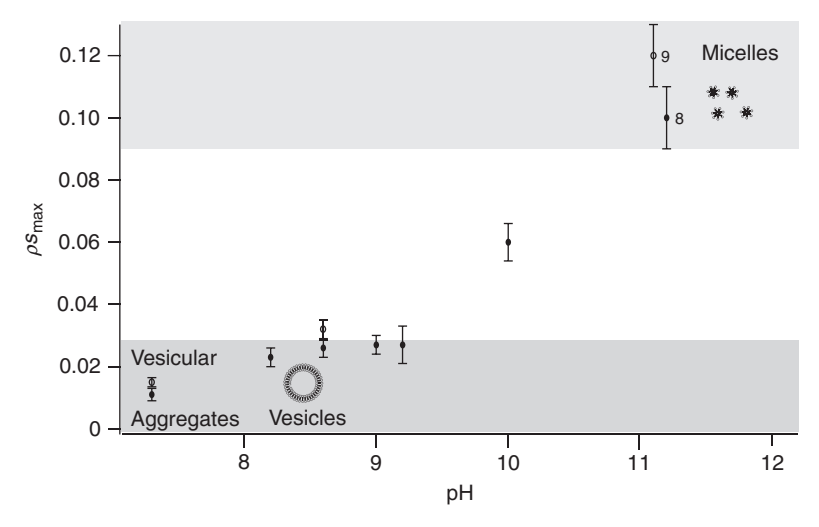


Figure 7 Plot of the change in the product of the coupling and maximum saturation factors as a function of macromolecular structure. At lower pH values, the spin-labelled lipids are present as vesicles and vesicular aggregates, while at higher pH values, micelles are formed. The higher $\rho s_{\rm max}$ values for the micelles imply greater water accessibility to the radical site. The solid circles represent 16-DS (16-doxyl stearic acid, spin-labelled at the end of the lipid tail) while the open circles represent 5-DS (5-doxyl stearic acid, spin-labelled near the polar head group). Reproduced with permission from Ref. [70].

molecules from the gel through heat-induced collapse. 127 This study was performed with imaging applications in mind, where the hyperpolarized solvent would no longer be in close contact with the radicals after the heat-induced collapse, giving enhanced signal with a longer T_1 relaxation time. These gels gave – 26-fold enhancement of water before heating, and the enhancement decreased with increasing temperature due to the gradual collapse of the gel. McCarney and Han⁵³ and Lingwood et al., ¹²⁴ on the other hand, measured the 0.35 T DNP enhancement of immobilized radicals for flow imaging applications, finding that TEMPO directly immobilized onto Sepharose beads gave $E_{\text{max}} = -46$, while TEMPO bound to a polyvinylimidazole polyelectrolyte linker which was then bound to Sepharose beads gave $E_{\text{max}} = -122$. While these systems are discussed in more detail in Section 3.5, it is appropriate to note here that spin-labelled polyelectrolytes have been observed to give the highest enhancements of all currently reported tethered nitroxide radical systems, with enhancement values approaching that of nitroxide radicals freely dissolved in solution.

This X-band Overhauser DNP technique has also been developed to study proteins and their interactions with site-specific resolution, employing site-directed mutagenesis and spin-labelling methods¹²⁸ to

introduce the spin label specifically at chosen protein sites. Pavlova et al. used tau proteins spin labelled at specific positions to demonstrate the utility of Overhauser DNP to monitor early protein aggregation events and observed the decrease of signal enhancement over the course of aggregation as the water was gradually slowed and ultimately excluded as protein monomers formed oligomers and eventually protein fibres. ^{56,84}

The majority of recent solution-state DNP studies at X-band have been focused on the hyperpolarization of ¹H signal. However, a recent report by Lingwood and Han described DNP signal enhancement of ¹³C-labelled small molecules dissolved in aqueous solution. ²⁴ The authors measured varying levels of signal enhancement from several small molecules and investigated the influence of the three-spin effect between the radical, the water proton and the ¹³C nuclei. They found that the relative levels of scalar and dipolar coupling are hard to predict for ¹³C, and showed that the three-spin effect can either increase or diminish the overall signal enhancement depending on whether scalar or dipolar enhancement is dominant. The authors concluded that the amount of DNP signal enhancement is more dependent on the distance of closest approach and the relative amounts of scalar and dipolar coupling, and not as dependent on the diffusion of the ¹³C-containing molecule.

Recently, reports on portable DNP instrumentation operating at X-band have appeared in the literature, made possible by recent advances in permanent magnet design and efficient solid-state X-band microwave amplifiers. Armstrong et al. described a portable system with a custombuilt microwave amplifier array capable of achieving greater than -100- fold DNP enhancement with 4-oxo-TEMPO radicals in water. 122 When combined with a variable-field Halbach magnet ($\sim\!0.3$ T) and a portable NMR spectrometer, the whole system fit easily onto a small cart. Lingwood et al. developed a portable DNP system using this microwave amplifier that was transported to a clinical MRI facility to perform DNP-enhanced flow imaging. 124 Münnemann et al. separately developed a mobile DNP system using a variable-field Halbach magnet at 0.30 T equipped with a cryostat and high-power travelling wave tube (TWT) microwave amplifier, which produced -50- fold enhancement using a spin-labelled cationic polyelectrolyte dissolved in a glycerol–water mixture. 123

Another report to mention is that of Toda et al., where they place an NMR coil directly above the microwave cavity of an X-band ESR system and shuttle the sample between the center of the microwave cavity and the NMR coil.³⁰ They observed – 19-fold enhancement with toluene and the BDPA radical at 0.40 T. Since their research program is focused on developing gyrotrons for high-field DNP, they did not further pursue X-band DNP experiments.

Finally, the application of optimal control theory to DNP studies needs to be discussed. Optimal control theory is a means to systematically design and optimize pulse sequences to maximize the efficiency of transfer between spin states. While this method was initially introduced to benefit high-resolution NMR studies, it has recently been adapted to improve the electron–nuclear polarization transfer in DNP applications by considering simple two- or three-spin systems. ^{129–131} While no experimental implementation of DNP pulse sequences designed by optimal control methods has been reported, these methods have the great potential to enhance DNP performance at X-band, due to the powerful pulsed ESR hardware that is commercially available at these frequencies.

3.4. High magnetic fields: Above 1 T

The reasons for performing DNP at higher magnetic fields are the same reasons why most conventional NMR studies benefit from higher fields: greater chemical shift resolution and higher (thermal) signal sensitivity. However, DNP at these fields suffers from the difficulty of generating, amplifying and efficiently transmitting the high ESR Larmor frequencies of tens and hundreds of gigahertz and from the high dielectric loss of electromagnetic radiation in liquid samples over this frequency regime. In spite of these difficulties, many researchers are pursuing DNP at fields above 1 T motivated by the great potential benefits of the technique.

The hardware required for DNP at high magnetic fields critically depends on the frequency required for ESR saturation. As the size of microwave resonators decreases with increasing frequency, simple resonant cavities like those used at X-band are not feasible at higher frequencies. Several microwave transmission systems have been reported: a horn and reflector at 40 GHz, ⁴⁰ a high-Q non-radiative dielectric resonator ¹³² and commercial ENDOR probes ^{41,133} at 95 GHz, an open waveguide and reflector at 140 GHz, ⁴⁶ a helical cavity at 260 GHz ¹³⁴ and a tapered waveguide and mirror at 300 GHz. ³⁰ Microwave sources employed for solution-state DNP also vary, including solid-state sources with TWT amplifiers at 40 GHz, ⁴⁰ unamplified ^{41,132} and amplified ¹³³ W-band bridges at 95 GHz, solid-state sources at 260 GHz ¹³⁴ and gyrotrons with frequency outputs ranging from 140 to 980 GHz. ^{30,46,135–138} Gyrotrons provide the highest power output by far of all sources listed here. Nearly all experimental systems in this range of fields utilize superconducting magnets.

Wind and Ardenkjær-Larsen reported the development of a 1.4 T DNP system using a horn and reflector system to transmit the 40 GHz radiation with a screening coil placed around the sample to reduce heating. ⁴⁰ Using a symmetric trityl radical, –9-fold enhancement of the water signal was measured in their report. In a second experiment, Wind et al. used the

same equipment to observe DNP with BDPA radicals dissolved in supercritical ethylene pressurized between 60 and 300 bar at room temperature. Scalar H Overhauser enhancements of up to E=55 were observed, caused by interactions between supercritical ethylene and undissolved BDPA, as BDPA was not appreciably soluble in supercritical ethylene. Also visible were small contributions from the solid/thermal mixing effect, implying that portions of ethylene were adsorbed to the solid radical surface for a prolonged time.

Several research groups have developed systems for DNP at 3.4 T based on W-band ESR equipment operating at 95 GHz. Annino et al. presented a novel double resonance structure for concurrent ESR saturation and NMR detection based on a high-Q non-radiative dielectric resonator with an integrated miniaturized radiofrequency coil. 132 With this design, an enhancement of E = -16 was measured for TEMPO dissolved in a mixture of water and dioxane with only 70 mW of microwave power. Villanueva-Garibay et al. used the same system to measure the DNP of TEMPO solutions in nanoliter volumes and observed even higher enhancements of up to E = -65 for 4-hydroxy-TEMPO dissolved in water. 43 This is much greater enhancement than expected at 95 GHz, based on theory and previous observations, and is likely due to the very high resonator quality factor and lossless penetration of radiation through the minute sample volume. Kryukov et al. developed a DNP spectrometer by using a commercial W-band ESR instrument with an ENDOR probe and inserting a high-power extended interaction klystron (EIK) amplifier into the system. 133 They measured -49-fold enhancements for toluene and 4-hydroxy-TEMPO, and performed extensive temperature dependence measurements to investigate the molecular motions in the system. Höfer et al. used an unmodified commercial ESR spectrometer and ENDOR cavity to carry out W-band DNP studies, and observed E = -20 for 4-hydroxy-TEMPO in water and E = -4 for a trityl radical.⁴¹ Türke et al. used the same system with a power upgrade module (400 mW) and found E = -43 for $^{15}N_{\star}^{16}D$ -4-oxo-TEMPO in water. Based on NMRD data from an accompanying paper, the authors give the coupling factor as $\rho = 0.11$. As it is apparent from this paragraph, DNP enhancement values and coupling factors measured at 95 GHz, even for the same radical and water system, widely diverge between different groups or experimental settings, while the same discussions for solutionstate DNP at X-band are nearing to a close agreement.

DNP in liquids has also been reported at higher fields of 5 T (140 GHz electron frequency) by Loening et al. ⁴⁶ In this report, the chemical systems were specifically selected to optimize scalar coupling, as the decrease in the coupling factor with increasing field is less dramatic for scalar-coupled species. ⁴ Enhancements of E=181 for ³¹P triphenylphospine, E=41 for ¹³C carbon tetrachloride, E=-35 for ¹⁵N aniline and E=9.4

for 19 F hexafluorobenzene were reported with BDPA employed as the radical. Note that the negative enhancements for 15 N are still due to scalar coupling, as the sign of enhancement is reversed due to the negative gyromagnetic ratio of 15 N.

Thus far, only one high-field DNP system operating at 9.2 T and 260 GHz has been reported to experimentally realize DNP enhancements of solution-state systems. The spectrometer design and ESR spectra were presented by Denysenkov et al., ¹³⁴ and the first DNP data were presented by Prandolini et al. ⁷⁹ This system gave E = -3.0 for 4-hydroxy-TEMPO in water, and the enhancement was confirmed to be due to the Overhauser effect with dipolar coupling. From here, the authors were able to achieve enhancements of E = -9.4 for water by improving microwave stability, increasing power to 45 mW from the previous 22 mW and by using ¹⁵N-Fremy's salt as a radical with higher DNP efficiency due to its narrower ESR linewidths. 72 Gafurov et al. investigated the biradical bis-TEMPObis-ketal, finding that the solution-state DNP enhancement of this radical at 9.2 T was entirely due to the Overhauser effect and that the -2- to -3fold enhancements from the biradical were similar to standard TEMPO radicals. 140 This instrument was also used to measure DNP enhancement as a function of microwave frequency, to compare with the results of the models developed by Sezer et al.⁵⁵ Most recently, the microwave source was replaced with a high-power gyrotron source (20 W) that led to a DNP enhancement of E = -28 for aqueous ¹⁵N-Fremy's salt at 60 °C. ¹³⁵

The work of researchers at the University of Fukui on developing high-power gyrotrons for DNP should be noted. They have recently reported the development of gyrotron microwave sources operating at 394 and 980 GHz and planned to apply these sources to DNP experiments at high fields. ^{136–138} DNP at 10.7 T and 300 GHz has also been attempted by the same authors, but the BDPA and toluene system completely evaporated due to sample heating before any NMR signal enhancement could be observed. ³⁰

Even though only a small number of reports have been published, it appears that the enhancement values measured so far at high magnetic fields are greater than what is predicted to be possible with existing theoretical models. Using the FFHS model and the reported translational correlation times for nitroxide radicals and water of $\tau_{\rm t}=20~{\rm ps},^{76}$ a coupling factor of 0.022 is derived for 260 GHz, which gives a maximum theoretical enhancement of $E_{\rm max}=-13.3$ (Equation (10) with f=1 and $s_{\rm max}=1$). This value is distinctly lower than the experimentally observed $E=-28,^{135}$ suggesting that different or new models may need to be considered and developed. For example, the rotational diffusion of individual water molecules with correlation times on the order of 1 ps may play a role. These discrepancies were the motivation for the development of MD simulations to calculate the coupling factor by Sezer et al. 35,55

However, it is clear overall that further detailed experimental studies and development of theory are necessary to enhance the current understanding of solution-state DNP at high magnetic fields.

3.5. DNP with flowing or shuttling between fields

One of the difficulties of designing a DNP experiment is simultaneously optimizing for high ESR saturation and sensitive NMR detection; however this can be partially overcome by hyperpolarizing and performing NMR detection at separate fields and rapidly transporting samples between the two locations and fields. This allows for the ESR saturation to be performed at a lower frequency to avoid the sample size restrictions found at higher irradiation frequencies and to avoid the complications of building NMR detection capabilities into a resonant microwave cavity. The NMR experiment can be performed at a higher field in a system designed for that purpose, offering greater sensitivity and often narrower NMR linewidths due to the presence of shim systems and the absence of bulky metal microwave components distorting the field homogeneity.

The downside of hyperpolarizing and detecting separately is that the enhanced signal decays with the T_1 value of the nuclei, and thus signal is lost during the shuttling process. This effect is dramatically increased if the radicals are left in contact with the sample during flow or shuttling, as an aqueous solution of radicals can easily have a $T_1 < 500$ ms for ^1H nuclei. In the case of ^{13}C or other nuclei such as ^{15}N or ^{29}Si , the transfer time should not be as significant due to the longer T_1 of those species. Alternately, immobilized radicals can be used for DNP, then filtered from the sample, 53,142,143 but previously described immobilized radical systems give lower DNP performance than radicals freely dissolved in solution. 53,63,127,143 However, a recent report describes the use of immobilized spin-labelled polyvinylimidazole for DNP studies, showing that this system gives DNP enhancement values approaching that of freely dissolved nitroxides with larger than -100-fold measured enhancements. 124

The idea of using flowing liquids with polarization highly amplified by Overhauser DNP was pioneered and developed by the Dorn group. In the first demonstration of the technique, the NMR coil was placed just below the microwave cavity in a commercial X-band ESR instrument; both hyperpolarization and detection were performed at 0.33 T and signal enhancements of approximately E=-64 were observed for benzene with the 2,4,6-tri-t-butylphenoxide radical. This experimental system was also used to demonstrate the feasibility of using immobilized radicals to hyperpolarize a flowing liquid by enhancing the signal of benzene flowing over spin-labelled silica gel. 143

The Dorn group then built a system to perform DNP at 0.33 T and detect NMR in a separate, higher field 4.7 T magnet, ¹⁴⁴ allowing for NMR

chemical shift resolution of the enhanced species. These low to high magnetic field transfer experiments necessitated the formulation of a new model for maximum enhancements by Tsai et al.,⁶² which included the effects of incomplete polarization build-up due to fast flow through the microwave cavity and the relaxation decay between hyperpolarization and NMR detection. Using this 0.33-4.7 T DNP system, different samples were investigated. In another paper by Tsai et al., dissolved TEMPO was used to enhance the ²⁹Si NMR signal of hexamethyldisiloxane. 82 Here, enhancement values of +13-fold were observed, which correspond to predominantly dipolar enhancement because the negative gyromagnetic ratio of ²⁹Si changes the sign of the enhanced signal. Dorn et al. investigated ¹³C DNP by using immobilized radicals to enhance benzene and chloroform, and noted a large (+63) scalar-dominated enhancement of chloroform. ⁶³ ¹³C DNP was also performed on fullerenes (C_{60}) dissolved in benzene using TEMPO radicals with the aim of describing collision dynamics in solution, where the enhancement for 20% ¹³C-labelled fullerenes was found to be dominated by dipolar coupling and mediated by mostly rotational motion. 145 Stevenson et al. further developed the flow-DNP technique as a detector for continuous-flow on-line chromatography, demonstrating greatly improved sensitivity for on-line ¹³C NMR detection after a chromatographic separation of several chlorinated and fluorinated organic molecules. ODNP was also shown to improve recycled-flow NMR experiments (the flowing sample brings new molecules into the NMR probe to shorten repetition times), where the DNP-enhanced experiments provided an increase in sensitivity over traditional, unenhanced recycled-flow NMR. 146 Most recently, Russ et al. used DNP, NMR contact shift measurements and density functional theory (DFT) calculations to investigate the collision dynamics of acetonitrile and acetamide using TEMPO radicals, finding that both molecules displayed dipolar and scalar coupling to the electron at different sites.²⁷

Reese, Krahn and co-workers have developed a shuttling system that allows for polarization at 0.34 T and NMR detection at 14.09 T. Their first design placed a 0.34 T permanent magnet directly above a 14 T superconducting magnet, employing a pneumatic shuttle system to transfer the sample in 115 ms. In the initial report, $^1\mathrm{H}$ enhancements of -0.41-fold (relative to thermal polarization at 14 T) were obtained with water and 4-hydroxy-TEMPO radicals. 147 The system was then optimized to provide enhancements of -2.6 for water and +15 for $^{13}\mathrm{C}$ chloroform, employing $^{15}\mathrm{N},^{16}\mathrm{D}\text{-}4\text{-}oxo\text{-}TEMPO$ radicals. 148 The second design of the shuttle system used ferromagnetic shims to modify the fringe field of the same 14 T magnet, thus allowing the placement of the hyperpolarization location inside the magnet bore and reducing the shuttle time to 40 ms. 149 With this system, $^{1}\mathrm{H}$ enhancements of -3.7 were measured for water using $^{15}\mathrm{N},^{16}\mathrm{D}\text{-}4\text{-}oxo\text{-}TEMPO$. Most importantly, the shorter shuttling time

allowed for the enhancement of molecules that were not detected with their earlier shuttling system because of rapid magnetization decay, including larger molecules. This finding was demonstrated with enhancements between -1.4 and -2.8 for the different protons of glucose.

The Han group has developed the hardware and techniques to enhance water at 0.35 T under continuous-flow, then subsequently image this hyperpolarized water either at 0.35 T or in higher fields, such as a 1.5 T. This technique, named remotely enhanced liquids for imaging contrast (RELIC), was first demonstrated by conducting both DNP and imaging experiments within a 0.35-T electromagnet. The flow dispersion path of enhanced water could clearly be visualized as it travelled through unenhanced bulk water—a phenomenon that cannot be visualized otherwise unless tracer molecules are used. As the hydrophilic, agarose gel-based immobilized radical systems were of a new design, they were described and characterized more thoroughly in a later report, with a maximum enhancement of $E_{\rm max} = -46.53$ This work was extended to a clinical setting, where efficient DNP enhancement was achieved in the 0.35 T location in the fringe field of a 1.5 T clinical MRI magnet that was modified to present sufficient field homogeneities using resistive shims. 124 The images at 1.5 T showed ¹H signal with -7-fold enhancement (relative to thermal polarization at 1.5 T), permitting direct visualization and tracing of enhanced water flow through a bulk water system. This is shown in Figure 8, where the trajectory of hyperpolarized water can easily be seen upon injection into a phantom filled with unenhanced water. While the fringe field of a 1.5 T magnet was used in this study, the authors note that the fringe field of non-actively shielded magnets up to \sim 4.7 T could be used, as the homogeneity requirements for DNP are much less than what is required for spectroscopy. This paper also includes the first report of an immobilized radical system that gives

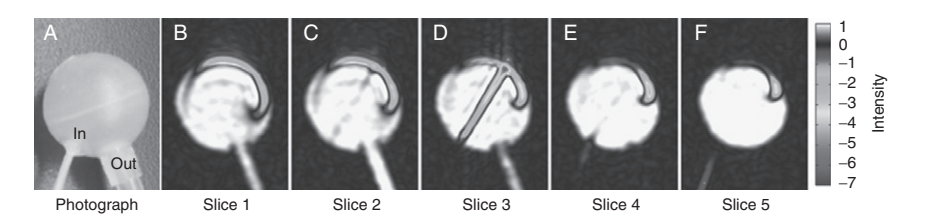


Figure 8 Photograph and MR images of a phantom for demonstrating the remotely enhanced liquids for imaging contrast (RELIC) technique. Water is hyperpolarized in the 0.35 T location in the fringe field then transferred into the center of the same magnet for imaging. (A) Photograph of the phantom; the water enters from the bottom left and exits through the bottom right. (B)–(F) Slices of the MR image with hyperpolarized water, clearly showing the jet of hyperpolarized water as it flows through unenhanced water. Adapted with permission from the full-color images in Ref. [124].

DNP enhancement approaching that of freely dissolved radicals, with the measured maximum enhancement of $E_{\rm max} = -122$ for immobilized spin-labelled polyvinylimidazole.

DNP has been performed in flowing systems to compare with CIDNP and stimulated nuclear polarization (SNP) experiments on radical reaction products. Here, the transfer from lower to higher fields was used for experimental convenience and was not the point of the work. Bagryanskaya et al. used polarization between 0 and 6 mT with detection at 4.7 T to study the mechanism of the photo-induced reactions of quinines 117 and the *trans-cis* isomerization of fumaronitrile. 118 Ananchenko et al. used the same system except with detection at 7 T to investigate the low-field transitions of the photolysis of 2,4,6-trimethylbenzoylphosphonic acid dimethyl ester. 119 These experiments were expanded by the work of Gorelik et al., where the theoretical basis of stationary and time-resolved DNP of reaction products was extended to include degenerated electron spin exchange, and the theory was compared with experiments. 120 Yamakage et al. utilized polarization at 0.33 T and detection at 2.35 T to investigate the photochemical reaction of benzaldehyde with time-resolved DNP, and describe a theoretical model suitable for these systems. 151 Most recently, Bagryanskaya et al. measured DNP and CIDNP of multiple radical reactions with polarization at 54 mT and 0.33 T accompanied with NMR detection at 7 T, and described the interplay of DNP, CIDNP and SNP that must be taken into account when investigating these systems. 121 The use of DNP to study radical reaction products in solution is a broad research area with many promising applications; however, a more thorough discussion is out of the scope of this review since this area has more in common with CIDNP (which employs a different mechanism) than conventional Overhauser DNP experiments where the goal is NMR signal enhancement.

The recent report of Korchak et al. describes a field-cycling DNP system which hyperpolarizes at either 10 or 49.6 mT with NMR detection at 7 T.⁹⁷ This paper is notable because the DNP was performed in the fringe field of the 7 T magnet. The aim of this report was to develop the theory for pulsed ESR saturation and optimize the experimental conditions such as pulse length, duty cycle, inter-pulse delay and applied power to give the greatest levels of DNP enhancement. By using pulsed ESR saturation, the authors were able to reduce applied ESR saturation power levels by a factor of 10 while only reducing observed enhancements by less than a factor of 2.

3.6. Proton-electron double resonance imaging

PEDRI (also known as Overhauser MRI) integrates the principles of Overhauser DNP with MRI to provide information on the spatial distribution of free radicals within the system of interest. Much work has been done to

develop PEDRI as an imaging modality, especially for *in vivo* applications; however, a complete collection of the large volume of PEDRI papers is out of the scope of this review. Instead, we describe the technical capabilities and recent applications of PEDRI and refer the reader to a number of recent reviews for further details. 44,152–157

PEDRI was first demonstrated by Lurie et al. in 1988¹⁵⁸ with phantom images at 40 mT (1.12 GHz electron saturation). This initial report was quickly followed by the introduction of field-cycled PEDRI. Because of the dielectric losses of biological samples, the magnetic field strengths used for electron saturation are limited to roughly 20 mT (\sim 560 MHz ESR frequency), with the optimum field value being somewhat lower. In avoid the low SNRs that occur when detecting nuclear signals at these low fields, field-cycling is now commonly combined with PEDRI experiments allowing for ESR saturation at lower fields and NMR/MRI detection at higher fields. SSR saturation at 5 mT and NMR detection at 450 mT.

PEDRI has been used for a number of different applications both in vitro and in vivo, where the in vivo experiments have thus only included animal models. The simplest example application is to monitor the distribution and clearance of the radical species in the body 160,167,168 or isolated organs¹⁶⁹ by comparing the amount of signal enhancement at different spatial locations, as shown in Figure 9. A common application of PEDRI is oximetry, where the amount of dissolved oxygen in vivo can be detected through the effects of paramagnetic oxygen on reducing observed DNP enhancements, due to reductions in the leakage factor and the lowering of ESR saturation of a broader ESR line. ^{156,170–174} Acidity can be measured *in* situ through pH-sensitive hyperfine ESR splittings of certain nitroxide radicals, where the DNP-detected ESR spectrum can easily be measured using field-cycled PEDRI instrumentation and recording signal enhancement as a function of magnetic field during electron saturation. 164,175,176 The progress of reduction/oxidation (redox) reactions can also be monitored with PEDRI through the consumption and regeneration of the unpaired electron (usually PROXYL radicals, 2,2,5,5-tetramethylpyrrolidine-N-oxyl) in the redox reaction, leading to the modulation of the DNP-enhanced ¹H NMR signal. ^{177–180} Proteolysis (protein degradation) information can be obtained with PEDRI through the use of spin-labelled proteins; when the spin-labelled protein is broken into small pieces during proteolysis, the nitroxide correlation time decreases and the DNP enhancement increases.¹⁸¹ Finally, systems have been developed to use Overhauser enhancements to assist with needle and catheter placement during interventional MRI, 182 including a self-contained 'marker' carrying a radical solution and coaxial transmission line for ESR saturation that can be inserted into tissue for locating the marker's enhanced signal with unmodified MRI equipment. 183,184

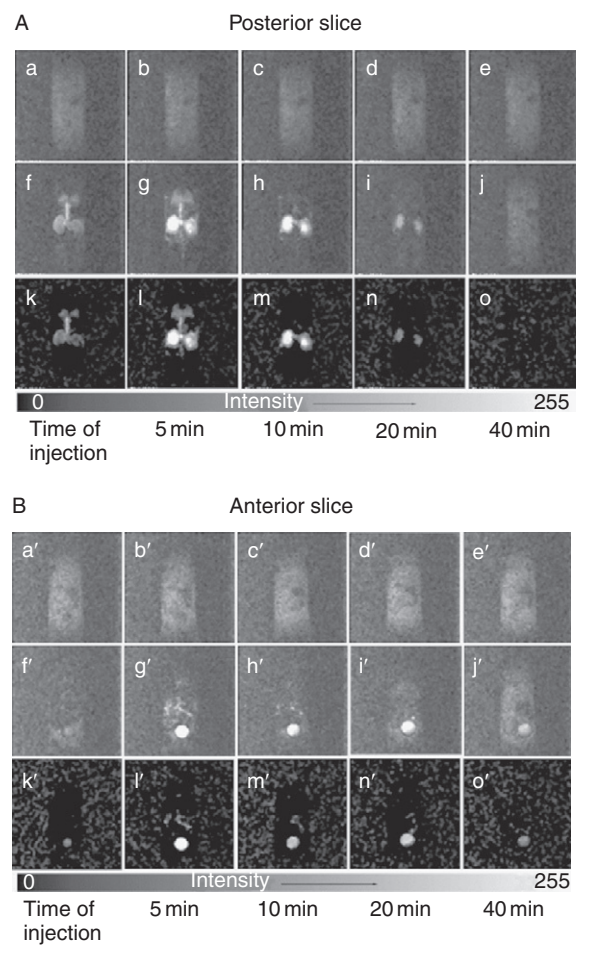


Figure 9 Time-dependent PEDRI images of a living mouse with an intravenous infusion of 2,2,5,5-tetramethyl-3-carboxylpyrrolidine-N-oxyl (PCA) radical. (A) The posterior slice: (a-e) no ESR irradiation, (f-j) 12 W of ESR irradiation and (k-o) the subtraction of ESR on and off images. (B) The anterior slice: (a'-e') no ESR irradiation, (f'-j') 12 W of ESR irradiation and (k'-o') the subtraction of ESR on and off images. The posterior images show that PCA is initially distributed in the heart, lungs, kidneys and major vessels, while the anterior images show that PCA is collected in the bladder over time. Adapted with permission from Ref. [160].

PEDRI is still an evolving field. In addition to application-oriented research, much emphasis is also being placed on improving the technique itself. Examples include the development of new field-cycling magnets, improved ESR saturation equipment and expanding the technique to include ¹⁹F detection. ^{187,188} Other new developments include

a real-time spectral analysis and visualization program, ¹⁸⁹ fast-imaging pulse sequences adapted to field-cycled PEDRI¹⁹⁰ and the implementation of intermolecular double-quantum coherence imaging. ¹⁹¹ As all these applications critically depend on the DNP performance of the radical species, some recent reports have focused on the characterization of existing radicals ³⁹ and the synthesis and DNP analysis of isotopically labelled radicals. ¹⁹² In addition to biological and *in vivo* studies, PEDRI has also been used to investigate the formation of hydrogels as a function of time ¹⁹³ and to monitor free radicals in sediment samples. ¹⁹⁴ The wide range of information accessible with PEDRI and the wide interest of the magnetic resonance community imply that much further research will be done in this area.

4. CONCLUSION

As has been presented in this review, there are many different applications and an exciting outlook for solution-state DNP techniques. While the Overhauser effect was first predicted over 50 years ago, DNP is still a young field due to the need for complex hardware and theory development. Much of the published work in this area has focused on developing the equipment and techniques and gaining an understanding of what is possible, rather than exploring or demonstrating applications and outcomes. The amount of interest in solution-state DNP has greatly increased over the past few years, and this is indicative of the great potential of the technique. Signal enhancement as the end goal is useful in portable and low-field applications, where the signal is difficult to detect without hyperpolarization. At higher fields, the contrast that is available through DNP is unique and specific to the local interactions between the radical and the solvent, and applications that exploit this specific contrast will provide insights in areas ranging from medical imaging to molecular interactions and interfaces. Reports of useful applications of Overhauser DNP methods have started to increase in the literature, many of which point towards the future of these techniques. If DNP is to transition from a curiosity into a mainstream experimental method, the information gained by DNP must be quantitative and made relevant to a broader scientific community. While there is still much work to be done, the great potential of solution-state Overhauser DNP indicates that these methods have a bright and promising future.

REFERENCES

- 1. A. W. Overhauser, Phys. Rev., 1953, 92, 411.
- 2. T. R. Carver and C. P. Slichter, Phys. Rev., 1953, 92, 212.
- 3. A. Abragam, Phys. Rev., 1955, 98, 1729.
- 4. K. H. Hausser and D. Stehlik, Adv. Magn. Reson., 1968, 3, 79.

- 5. A. Abragam and M. Goldman, Rep. Prog. Phys., 1978, 41, 395.
- R. A. Wind, M. J. Duijvestijn, C. van der Lugt, A. Manenschijn and J. Vriend, Prog. Nucl. Magn. Reson. Spectrosc., 1985, 17, 33.
- C. T. Farrar, D. A. Hall, G. J. Gerfen, S. J. Inati and R. G. Griffin, J. Chem. Phys., 2001, 114, 4922.
- J. H. Ardenkjær-Larsen, B. Fridlund, A. Gram, G. Hansson, L. Hansson, M. H. Lerche, R. Servin, M. Thaning and K. Golman, *Proc. Natl. Acad. Sci. USA*, 2003, 100, 10158.
- A. B. Barnes, G. De Paëpe, P. C. A. van der Wel, K. N. Hu, C. G. Joo, V. S. Bajaj, M. L. Mak-Jurkauskas, J. R. Sirigiri, J. Herzfeld, R. J. Temkin and R. G. Griffin, *Appl. Magn. Reson.*, 2008, 34, 237.
- T. Maly, G. T. Debelouchina, V. S. Bajaj, K.-N. Hu, C.-G. Joo, M. L. MakJurkauskas, J. R. Sirigiri, P. C. A. van der Wel, J. Herzfeld, R. J. Temkin and R. G. Griffin, J. Chem. Phys., 2008, 128, 052211.
- 11. C. G. Joo, A. Casey, C. J. Turner and R. G. Griffin, J. Am. Chem. Soc., 2009, 131, 12.
- 12. C.-G. Joo, K.-N. Hu, J. A. Bryant and R. G. Griffin, J. Am. Chem. Soc., 2006, 128, 9428.
- 13. F. A. Gallagher, M. I. Kettunen and K. M. Brindle, Prog. Nucl. Magn. Reson. Spectrosc., 2009, 55, 285.
- 14. K. Golman and J. S. Petersson, Acad. Radiol., 2006, 13, 932.
- 15. J. R. Woodward, Prog. React. Kinet. Mech., 2002, 27, 165.
- M. Goez, Photo-CIDNP spectroscopy. in: Annual Reports on NMR Spectroscopy, (G. A. Webb ed.). Academic Press, London, 2009, 66, pp. 77–147.
- 17. J. Matysik, A. Diller, E. Roy and A. Alia, Photosynth. Res., 2009, 102, 427.
- 18. G. Kaur and G. Denninger, Appl. Magn. Reson., 2010, 39, 185.
- S. B. Orlinskii, J. Schmidt, P. G. Baranov, C. d. M. Donegá and A. Meijerink, *Phys. Rev. B*, 2009, **79**, 165316.
- 20. R. D. Bates, Magn. Reson. Rev., 1993, 16, 237.
- 21. W. Müller-Warmuth and K. Meise-Gresch, Adv. Magn. Reson., 1983, 11, 1.
- 22. J. Potenza, Adv. Mol. Relax. Process, 1972, 4, 229.
- 23. C. P. Slichter, Principles of Magnetic Resonance. Springer-Verlag, Berlin, 1990.
- 24. M. D. Lingwood and S. Han, J. Magn. Reson., 2009, 201, 137.
- 25. A. Abragam, The Principles of Nuclear Magnetism. Clarendon Press, Oxford, 1961.
- 26. B. D. Armstrong and S. Han, J. Am. Chem. Soc., 2009, 131, 4641.
- J. L. Russ, J. Gu, K.-H. Tsai, T. Glass, J. C. Duchamp and H. C. Dorn, J. Am. Chem. Soc., 2007, 129, 7018.
- 28. I. Solomon, Phys. Rev., 1955, 99, 559.
- 29. P. Höfer, P. Carl, G. Guthausen, T. Prisner, M. Reese, T. Carlomagno, C. Griesinger and M. Bennati, *Appl. Magn. Reson.*, 2008, **34**, 393.
- 30. M. Toda, Y. Fujii, S. Mitsudo, I. Ogawa, T. Idehara, T. Saito, H. Ito and M. Chiba, Appl. Magn. Reson., 2008, 34, 277.
- 31. R. D. Bates and W. S. Drozdoski, J. Chem. Phys., 1977, 67, 4038.
- 32. A. O. Salman, M. M. Sünnetçioğlu, R. Sungur and G. Bingöl, J. Magn. Reson., 1998, 134, 1.
- 33. H. C. Dorn, J. Wang, L. Allen, D. Sweeney and T. E. Glass, J. Magn. Reson., 1988, 79, 404.
- B. M. Odintsov, R. L. Belford, P. J. Ceroke, A. B. Odintsov and R. B. Clarkson, *Surf. Sci.*, 1997, 393, 162.
- 35. D. Sezer, M. J. Prandolini and T. F. Prisner, Phys. Chem. Chem. Phys., 2009, 11, 6626.
- 36. T. Guiberteau and D. Grucker, J. Magn. Reson. B, 1996, 110, 47.
- 37. D. Grucker, T. Guiberteau, B. Eclancher, J. Chambron, R. Chiarelli, A. Rassat, G. Subra and B. Gallez, *J. Magn. Reson. B*, 1995, **106**, 101.
- 38. D. J. Lurie, I. Nicholson and J. R. Mallard, J. Magn. Reson., 1991, 94, 197.
- A. M. F. Benial, K. Ichikawa, R. Murugesan, K. I. Yamada and H. Utsumi, J. Magn. Reson., 2006, 182, 273.
- 40. R. A. Wind and J.-H. Ardenkjær-Larsen, J. Magn. Reson., 1999, 141, 347.

- 41. P. Höfer, G. Parigi, C. Luchinat, P. Carl, G. Guthausen, M. Reese, T. Carlomagno, C. Griesinger and M. Bennati, *J. Am. Chem. Soc.*, 2008, **130**, 3254.
- 42. B. M. Odintsov, R. L. Belford and R. B. Clarkson, J. Phys. Chem. A, 1997, 101, 116.
- J. A. Villanueva-Garibay, G. Annino, P. J. M. van Bentum and A. P. M. Kentgens, *Phys. Chem. Chem. Phys.*, 2010, 12, 5846.
- K. Golman, I. Leunbach, J. H. Ardenkjær-Larsen, G. J. Ehnholm, L. G. Wistrand, J. S. Petersson, A. Järvi and S. Vahasalo, *Acta Radiol.*, 1998, 39, 10.
- 45. D. Neuhaus and M. P. Williamson, The Nuclear Overhauser Effect in Structural and Conformational Analysis. Wiley-VCH, New York, 2000.
- 46. N. M. Loening, M. Rosay, V. Weis and R. G. Griffin, J. Am. Chem. Soc., 2002, 124, 8808.
- 47. O. H. Griffith, D. W. Cornell and H. M. McConnell, J. Chem. Phys., 1965, 43, 2909.
- 48. T. J. Stone, T. Buckman, P. L. Nordio and H. M. McConnell, *Proc. Natl. Acad. Sci. USA*, 1965, **54**, 1010.
- 49. I. Nicholson, D. J. Lurie and F. J. L. Robb, J. Magn. Reson. B, 1994, 104, 250.
- 50. B. D. Armstrong and S. Han, J. Chem. Phys., 2007, 127, 104508.
- 51. J. M. Franck, A. Pavlova and S. Han, Prog. Nucl. Magn. Reson. Spectrosc., (in preparation).
- 52. B. H. Robinson, D. A. Haas and C. Mailer, Science, 1994, 263, 490.
- 53. E. R. McCarney and S. Han, J. Magn. Reson., 2008, 190, 307.
- 54. M. Goldman, J. Magn. Reson., 2001, 149, 160.
- D. Sezer, M. Gafurov, M. J. Prandolini, V. P. Denysenkov and T. F. Prisner, *Phys. Chem. Chem. Phys.*, 2009, 11, 6638.
- A. Pavlova, E. R. McCarney, D. W. Peterson, F. W. Dahlquist, J. Lew and S. Han, Phys. Chem. Chem. Phys., 2009, 11, 6833.
- 57. B. Borah and R. G. Bryant, J. Chem. Phys., 1981, 75, 3297.
- W. Müller-Warmuth, R. Vilhjalmsson, P. A. M. Gerlof, J. Smidt and J. Trommel, Mol. Phys., 1976, 31, 1055.
- 59. H. Brunner and K. H. Hausser, J. Magn. Reson., 1972, 6, 605.
- 60. S. Stevenson and H. C. Dorn, Anal. Chem., 1994, 66, 2993.
- 61. K. H. Hausser and F. Reinbold, Phys. Lett., 1962, 2, 53.
- 62. K. H. Tsai and H. C. Dorn, Appl. Magn. Reson., 1990, 1, 231.
- 63. H. Dorn, T. Glass, R. Gitti and K. Tsai, Appl. Magn. Reson., 1991, 2, 9.
- J. H. Ardenkjær-Larsen, I. Laursen, I. Leunbach, G. Ehnholm, L. G. Wistrand, J. S. Petersson and K. Golman, J. Magn. Reson., 1998, 133, 1.
- 65. J. H. Freed, J. Chem. Phys., 1978, 68, 4034.
- 66. L.-P. Hwang and J. H. Freed, J. Chem. Phys., 1975, 63, 4017.
- 67. R. Kausik and S. Han, J. Am. Chem. Soc., 2009, 131, 18254.
- S. Garcia, J. H. Walton, B. Armstrong, S. Han and M. J. McCarthy, J. Magn. Reson., 2010, 203, 138.
- R. Kausik, A. Srivastava, P. A. Korevaar, G. Stucky, J. H. Waite and S. Han, Macromolecules, 2009, 42, 7404.
- 70. E. R. McCarney, B. D. Armstrong, R. Kausik and S. Han, Langmuir, 2008, 24, 10062.
- M. T. Türke, I. Tkach, M. Reese, P. Höfer and M. Bennati, *Phys. Chem. Chem. Phys.*, 2010, 12, 5893.
- M. J. Prandolini, V. P. Denysenkov, M. Gafurov, B. Endeward and T. F. Prisner, J. Am. Chem. Soc., 2009, 131, 6090.
- 73. B. D. Armstrong, P. Soto, J.-E. Shea and S. Han, J. Magn. Reson., 2009, 200, 137.
- É. Tóth, L. Helm and A. Merbach, Relaxivity of MRI contrast agents. in: Contrast Agents I, (W. Krause ed.). Springer, Berlin/Heidelberg, 2002.
- M. W. Hodges, D. S. Cafiso, C. F. Polnaszek, C. C. Lester and R. G. Bryant, *Biophys. J.*, 1997, 73, 2575.
- M. Bennati, C. Luchinat, G. Parigi and M. T. Türke, Phys. Chem. Chem. Phys., 2010, 12, 5902.

- 77. C. Luchinat and G. Parigi, Appl. Magn. Reson., 2008, 34, 379.
- 78. B. Halle, J. Chem. Phys., 2009, 131, 224507.
- 79. M. J. Prandolini, V. P. Denysenkov, M. Gafurov, S. Lyubenova, B. Endeward, M. Bennati and T. F. Prisner, *Appl. Magn. Reson.*, 2008, **34**, 399.
- 80. A. Peksoz, M. A. Çimenoğlu and A. Yalçiner, J. Disper. Sci. Technol., 2008, 29, 40.
- 81. A. Peksoz, A. Yalçiner and M. A. Çimenoğlu, Z. Naturforsch. A, 2009, 64, 477.
- 82. K. H. Tsai, T. E. Glass and H. C. Dorn, J. Magn. Reson., 1990, 89, 362.
- 83. I. Sert, M. M. Sünnetçioğlu, R. Sungur and G. Bingöl, Z. Naturforsch. A, 2000, 55, 682.
- 84. J. H. Ortony, C.-Y. Cheng, J. M. Franck, R. Kausik, A. Pavlova, J. Hunt and S. Han, *New J. Phys.*, 2011, **13**, 015006.
- 85. T. R. Carver and C. P. Slichter, Phys. Rev., 1956, 102, 975.
- 86. L. H. Bennett and H. C. Torrey, Phys. Rev., 1957, 108, 499.
- 87. M. D. Lingwood, I. A. Ivanov, A. R. Cote and S. Han, J. Magn. Reson., 2010, 204, 56.
- 88. T. Guiberteau and D. Grucker, J. Magn. Reson. A, 1993, 105, 98.
- 89. H. Ovalioğlu, A. Peksoz, H. E. Kırımlı and A. Yalçiner, Z. Naturforsch. A, 2010, 65, 254.
- 90. G. Breit and I. I. Rabi, Phys. Rev., 1931, 38, 2082.
- 91. V. W. Müller-Warmuth, Z. Naturforsch., 1960, 15a, 927.
- 92. R. D. Bates, J. Magn. Reson., 1982, 48, 111.
- 93. C. Polyon, D. J. Lurie, W. Youngdee, C. Thomas and I. Thomas, J. Phys. D, 2007, 40, 5527.
- 94. M. Fedin, S. Shakirov, P. Purtov and E. Bagryanskaya, Russ. Chem. Bull., 2006, 55, 1703.
- 95. D. M. TonThat, M. P. Augustine, A. Pines and J. Clarke, Rev. Sci. Instrum., 1997, 68, 1527.
- 96. N. Zeghib and D. Grucker, Phys. Med. Biol., 2001, 46, 2371.
- 97. S. E. Korchak, A. S. Kiryutin, K. L. Ivanov, A. V. Yurkovskaya, Y. A. Grishin, H. Zimmermann and H. M. Vieth, *Appl. Magn. Reson.*, 2010, **37**, 515.
- 98. M. E. Halse and P. T. Callaghan, J. Magn. Reson., 2008, 195, 162.
- 99. D. J. Lurie, I. Nicholson and J. R. Mallard, J. Magn. Reson., 1991, 95, 405.
- 100. V. A. Sapunov and A. K. Chirkov, Sov. J. Chem. Phys., 1991, 7, 1447.
- 101. A. Y. Tregubenkov and V. I. Baldin, Sov. J. Chem. Phys., 1991, 7, 1238.
- 102. A. Y. Tregubenkov, V. I. Baldin and S. P. Dovgopol, Teor. Eksp. Khim., 1991, 27, 1.
- 103. M. Alecci and D. J. Lurie, J. Magn. Reson., 1999, 138, 313.
- 104. M. Sünnetçioğlu, G. Bingöl and R. Sungur, Z. Naturforsch. A, 1991, 46, 976.
- 105. R. Sungur, Doga Turk. Fiz. Astrofiz. Derg., 1991, 15, 63.
- 106. N. Horasan, M. M. Sünnetçioğlu, R. Sungur and G. Bingöl, Z. Naturforsch. A, 1997, 52,
- 107. C. Akay and A. Yalçiner, Z. Naturforsch. A, 1995, 50, 177.
- 108. M. A. Çimenoğlu, Fuel, 2001, 80, 2041.
- 109. D. Aydoğdu, M. A. Çimenoğlu and A. Yalçiner, J. Disper. Sci. Technol., 2006, 27, 955.
- 110. N. U. Ersözlü, A. Peksöz, H. Ovalıoğlu, H. E. Kırımlı, M. A. Çimenoğlu and A. Yalçiner, *J. Disper. Sci. Technol.*, 2008, **29**, 899.
- 111. H. Ovalioğlu, A. Peksoz, H. E. Kırımlı and A. Yalçiner, J. Disper. Sci. Technol., 2010, 31, 332.
- B. M. Odintsov, R. L. Belford, P. J. Ceroke and R. B. Clarkson, J. Am. Chem. Soc., 1998, 120, 1076.
- 113. R. B. Clarkson, B. M. Odintsov, P. J. Ceroke, J. H. Ardenkjær-Larsen, M. Fruianu and R. L. Belford, *Phys. Med. Biol.*, 1907, 1998, 43.
- 114. B. M. Odintsov, R. L. Belford, P. J. Ceroke, Z. S. Idiyatullin, R. S. Kashaev, I. V. Kuriashkin, V. S. Rukhlov, A. N. Temnikov and R. B. Clarkson, J. Magn. Reson., 1998, 135, 435.
- 115. N. Kernevez and H. Glénat, IEEE Trans. Magn., 1991, 27, 5402.
- 116. D. I. Hoult and R. E. Richards, J. Magn. Reson., 1976, 24, 71.
- 117. E. G. Bagryanskaya, Y. A. Grishin, N. I. Avdievitch, R. Z. Sagdeev and Y. N. Molin, *Chem. Phys. Lett.*, 1986, **128**, 162.

- 118. E. G. Bagryanskaya, N. I. Avdievich, Y. A. Grishin and R. Z. Sagdeev, *Chem. Phys.*, 1989, 135, 123.
- G. S. Ananchenko, E. G. Bagryanskaya and R. Z. Sagdeev, Chem. Phys. Lett., 1998, 282, 450.
- 120. V. R. Gorelik, E. G. Bagryanskaya, N. N. Lukzen, I. V. Koptyug, V. V. Perov and R. Z. Sagdeev, *J. Phys. Chem.*, 1996, **100**, 5800.
- 121. E. G. Bagryanskaya, G. S. Ananchenko, T. Nagashima, K. Maeda, S. Milikisyants and H. Paul, J. Phys. Chem. A, 1999, 103, 11271.
- 122. B. D. Armstrong, M. D. Lingwood, E. R. McCarney, E. R. Brown, P. Blümler and S. Han, *J. Magn. Reson.*, 2008, **191**, 273.
- 123. K. Münnemann, C. Bauer, J. Schmiedeskamp, H. W. Spiess, W. G. Schreiber and D. Hinderberger, *Appl. Magn. Reson.*, 2008, **34**, 321.
- 124. M. D. Lingwood, T. A. Siaw, N. Sailasuta, B. D. Ross, P. Bhattacharya and S. Han, *J. Magn. Reson.*, 2010, **205**, 247.
- 125. S. Han, E. R. McCarney and B. D. Armstrong, Appl. Magn. Reson., 2008, 34, 439.
- 126. S. Han, E. R. McCarney, B. D. Armstrong and M. D. Lingwood, Dynamic nuclear polarization-enhanced magnetic resonance analysis at X-band using amplified ¹H water signal. *in*: Magnetic Resonance Microscopy, S. L. Codd and J. D. Seymour (eds.), . Wiley-VCH, Weinheim, 2009.
- 127. B. C. Dollmann, M. J. N. Junk, M. Drechsler, H. W. Spiess, D. Hinderberger and K. Münnemann, *Phys. Chem. Chem. Phys.*, 2010, **12**, 5879.
- 128. W. L. Hubbell and C. Altenbach, Curr. Opin. Struct. Biol., 1994, 4, 566.
- 129. N. Pomplun, B. Heitmann, N. Khaneja and S. J. Glaser, Appl. Magn. Reson., 2008, 34, 331.
- 130. N. Pomplun and S. J. Glaser, Phys. Chem. Chem. Phys., 2010, 12, 5791.
- 131. I. I. Maximov, Z. Tošner and N. C. Nielsen, J. Chem. Phys., 2008, 128, 184505.
- 132. G. Annino, J. A. Villanueva-Garibay, P. J. M. van Bentum, A. A. K. Klaassen and A. P. M. Kentgens, *Appl. Magn. Reson.*, 2010, 37, 851.
- 133. E. V. Kryukov, M. E. Newton, K. J. Pike, D. R. Bolton, R. M. Kowalczyk, A. P. Howes, M. E. Smith and R. Dupree, *Phys. Chem. Chem. Phys.*, 2010, **12**, 5757.
- 134. V. P. Denysenkov, M. J. Prandolini, A. Krahn, M. Gafurov, B. Endeward and T. F. Prisner, *Appl. Magn. Reson.*, 2008, **34**, 289.
- 135. V. Denysenkov, M. J. Prandolini, M. Gafurov, D. Sezer, B. Endeward and T. F. Prisner, *Phys. Chem. Chem. Phys.*, 2010, **12**, 5786.
- 136. T. Idehara, K. Kosuga, L. Agusu, R. Ikeda, I. Ogawa, T. Saito, Y. Matsuki, K. Ueda and T. Fujiwara, *J. Infrared Millim. Te.*, 2010, **31**, 775.
- 137. T. Idehara, T. Saito, I. Ogawa, S. Mitsudo, Y. Tatematsu, L. Agusu, H. Mori and S. Kobayashi, *Appl. Magn. Reson.*, 2009, **34**, 265.
- 138. S. P. Sabchevski and T. Idehara, J. Infrared Millim. Te., 2010, 31, 934.
- R. A. Wind, S. Bai, J. Z. Hu, M. S. Solum, P. D. Ellis, D. M. Grant, R. J. Pugmire, C. M. V. Taylor and C. R. Yonker, *J. Magn. Reson.*, 2000, 143, 233.
- 140. M. Gafurov, S. Lyubenova, V. Denysenkov, O. Ouari, H. Karoui, F. Le Moigne, P. Tordo and T. Prisner, *Appl. Magn. Reson.*, 2010, **37**, 505.
- 141. B. Halle and L. Nilsson, J. Phys. Chem. B, 2009, 113, 8210.
- 142. H. H. Fischer, M. Seiler, T. S. Ertl, U. Eberhardinger, H. Bertagnolli, H. Schmitt-Willich and K. Albert, *J. Phys. Chem. B*, 2003, **107**, 4879.
- R. Gitti, C. Wild, C. Tsiao, K. Zimmer, T. E. Glass and H. C. Dorn, J. Am. Chem. Soc., 1988, 110, 2294.
- 144. H. C. Dorn, R. Gitti, K. H. Tsai and T. E. Glass, Chem. Phys. Lett., 1989, 155, 227.
- H. C. Dorn, J. Gu, D. S. Bethune, R. D. Johnson and C. S. Yannoni, *Chem. Phys. Lett.*, 1993, 203, 549.
- 146. S. Stevenson, T. Glass and H. C. Dorn, Anal. Chem., 1998, 70, 2623.

- M. Reese, D. Lennartz, T. Marquardsen, P. Höfer, A. Tavernier, P. Carl, T. Schippmann, M. Bennati, T. Carlomagno, F. Engelke and C. Griesinger, *Appl. Magn. Reson.*, 2008, 34, 301.
- M. Reese, M.-T. Türke, I. Tkach, G. Parigi, C. Luchinat, T. Marquardsen, A. Tavernier,
 P. Höfer, F. Engelke, C. Griesinger and M. Bennati, J. Am. Chem. Soc., 2009, 131, 15086.
- 149. A. Krahn, P. Lottmann, T. Marquardsen, A. Tavernier, M. T. Türke, M. Reese, A. Leonov, M. Bennati, P. Hoefer, F. Engelke and C. Griesinger, *Phys. Chem. Chem. Phys.*, 2010, 12, 5830.
- E. R. McCarney, B. D. Armstrong, M. D. Lingwood and S. Han, *Proc. Natl. Acad. Sci. USA*, 2007, **104**, 1754.
- 151. Y. Yamakage, K. Maeda and T. Azumi, Mol. Phys., 1997, 90, 431.
- D. J. Lurie, S. Aime, S. Baroni, N. A. Booth, L. M. Broche, C. H. Choi, G. R. Davies,
 S. Ismail, D. O. hÓgáin and K. J. Pine, C. R. Phys., 2010, 11, 136.
- 153. K. I. Matsumoto, S. Subramanian, R. Murugesan, J. B. Mitchell and M. C. Krishna, *Antioxid. Redox Signal.*, 2007, **9**, 1125.
- 154. D. J. Lurie and K. Mäder, Adv. Drug Deliv. Rev., 2005, 57, 1171.
- 155. B. Gallez, C. Baudelet and B. F. Jordan, NMR Biomed., 2004, 17, 240.
- 156. M. C. Krishna, S. Subramanian, P. Kuppusamy and J. B. Mitchell, Semin. Radiat. Oncol., 2001, 11, 58.
- 157. D. Grucker, Prog. Nucl. Magn. Reson. Spectrosc., 2000, 36, 241.
- 158. D. J. Lurie, D. M. Bussell, L. H. Bell and J. R. Mallard, J. Magn. Reson., 1988, 76, 366.
- D. J. Lurie, J. M. S. Hutchison, L. H. Bell, I. Nicholson, D. M. Bussell and J. R. Mallard, J. Magn. Reson., 1989, 84, 431.
- 160. H. Li, G. He, Y. Deng, P. Kuppusamy and J. L. Zweier, Magn. Reson. Med., 2006, 55, 669.
- 161. W. Youngdee, G. Planinšič and D. J. Lurie, Phys. Med. Biol., 2001, 46, 2531.
- 162. G. Planinšič, T. Guiberteau and D. Grucker, J. Magn. Reson. B, 1996, 110, 205.
- 163. T. Claasen-Vujčić, H. Borsboom, E. Konijnenburg, D. Korbee, J. Trommel and T. Mehlkopf, *Phys. Med. Biol.*, 1863, 1998, 43.
- 164. V. V. Khramtsov, G. L. Caia, K. Shet, E. Kesselring, S. Petryakov, J. L. Zweier and A. Samouilov, J. Magn. Reson., 2010, 202, 267.
- 165. K. Shet, G. L. Caia, E. Kesselring, A. Samouilov, S. Petryakov, D. J. Lurie and J. L. Zweier, J. Magn. Reson., 2010, 205, 202.
- 166. D. J. Lurie, G. R. Davies, M. A. Foster and J. M. S. Hutchison, *Magn. Reson. Imaging*, 2005, 23, 175.
- H. Li, Y. Deng, G. He, P. Kuppusamy, D. J. Lurie and J. L. Zweier, Magn. Reson. Med., 2002, 48, 530.
- 168. K. Golman, I. Leunbach, J. S. Petersson, D. Holz and J. Overweg, *Acad. Radiol.*, 2002, 9, S104.
- 169. T. Liebgott, H. Li, Y. Deng and J. L. Zweier, Magn. Reson. Med., 2003, 50, 391.
- 170. S. Matsumoto, H. Yasui, S. Batra, Y. Kinoshita, M. Bernardo, J. P. Munasinghe, H. Utsumi, R. Choudhuri, N. Devasahayam, S. Subramanian, J. B. Mitchell and M. C. Krishna, *Proc. Natl. Acad. Sci. USA*, 2009, 106, 17898.
- 171. S. Matsumoto, H. Utsumi, T. Aravalluvan, K. Matsumoto, A. Matsumoto, N. Devasahayam, A. L. Sowers, J. B. Mitchell, S. Subramanian and M. C. Krishna, Magn. Reson. Med., 2005, 54, 213.
- 172. S. Subramanian, K.-i. Matsumoto, J. B. Mitchell and M. C. Krishna, NMR Biomed., 2004, 17, 263.
- 173. M. C. Krishna, S. English, K. Yamada, J. Yoo, R. Murugesan, D. Nallathamby, J. A. Cook, K. Golman, J. H. Ardenkjaer-Larsen, S. Subramanian and J. B. Mitchell, *Proc. Natl. Acad. Sci. USA*, 2002, **99**, 2216.
- 174. K. Golman, J. S. Petersson, J.-H. Ardenkjær-Larsen, I. Leunbach, L.-G. Wistrand, G. Ehnholm and K. Liu, J. Magn. Reson. Imaging, 2000, 12, 929.

- 175. D. I. Potapenko, M. A. Foster, D. J. Lurie, I. A. Kirilyuk, J. M. S. Hutchison, I. A. Grigor'ev, E. G. Bagryanskaya and V. V. Khramtsov, J. Magn. Reson., 2006, 182, 1.
- M. A. Foster, I. A. Grigor'ev, D. J. Lurie, V. V. Khramtsov, S. McCallum, I. Panagiotelis, J. M. S. Hutchison, A. Koptioug and I. Nicholson, Magn. Reson. Med., 2003, 49, 558.
- 177. A. M. F. Benial, H. Utsumi, K. Ichikawa, R. Murugesan, K.-i. Yamada, Y. Kinoshita, T. Naganuma and M. Kato, *J. Magn. Reson.*, 2010, **204**, 131.
- 178. M. Yamato, T. Shiba, K. Yamada, T. Watanabe and H. Utsumi, J. Cereb. Blood Flow Met., 2009, 29, 1655.
- 179. F. Hyodo, R. Murugesan, K.-i. Matsumoto, E. Hyodo, S. Subramanian, J. B. Mitchell and M. C. Krishna, *J. Magn. Reson.*, 2008, **190**, 105.
- 180. H. Utsumi, K. Yamada, K. Ichikawa, K. Sakai, Y. Kinoshita, S. Matsumoto and M. Nagai, Proc. Natl. Acad. Sci. USA, 2006, 103, 1463.
- 181. P. Mellet, P. Massot, G. Madelin, S. R. A. Marque, E. Harte, J. M. Franconi and E. Thiaudière, *PLoS ONE*, 2009, 4, 9.
- 182. E. Vahala, M. Ylihautala, G. Ehnholm, N. Etelä, I. Young, K. Golman and I. Leunbach, J. Magn. Reson., 2002, 157, 298.
- 183. R. P. Joensuu, R. E. Sepponen, A. E. Lamminen and C.-G. M. Standertskjöld-Nordenstam, *Magn. Reson. Med.*, 2000, **43**, 139.
- 184. R. P. J. Joensuu, R. E. Sepponen, A. E. Lamminen and C.-G. M. Standertskjöld-Nordenstam, *Acta Radiol.*, 1997, **38**, 43.
- 185. S. Matsumoto, K. Yamada, H. Hirata, K. Yasukawa, F. Hyodo, K. Ichikawa and H. Utsumi, *Magn. Reson. Med.*, 2007, **57**, 806.
- S. Petryakov, A. Samouilov, M. Roytenberg, H. H. Li and J. L. Zweier, Magn. Reson. Med., 2006, 56, 654.
- 187. A. Modica, D. J. Lurie and M. Alecci, Phys. Med. Biol., 2006, 51, N39.
- 188. R. Murugesan, S. English, K. Reijnders, K.-i. Yamada, J. A. Cook, J. B. Mitchell, S. Subramanian and M. C. Krishna, *Magn. Reson. Med.*, 2002, **48**, 523.
- 189. Y. Deng, K. Shet, H. Li, P. Kuppusamy and J. L. Zweier, Comput. Methods Programs Biomed., 2006, 82, 67.
- 190. W. Youngdee, D. J. Lurie and M. A. Foster, Phys. Med. Biol., 2002, 47, 1091.
- 191. W. Barros, P. L. de Sousa and M. Engelsberg, J. Magn. Reson., 2003, 165, 175.
- 192. K. I. Yamada, Y. Kinoshita, T. Yamasaki, H. Sadasue, F. Mito, M. Nagai, S. Matsumoto, M. Aso, H. Suemune, K. Sakai and H. Utsumi, *Arch. Pharm.*, 2008, **341**, 548.
- 193. J. W. Barros and M. Engelsberg, J. Magn. Reson., 2007, 184, 101.
- 194. N. Nestle, K. Shet and D. J. Lurie, Magn. Reson. Imaging, 2005, 23, 183.